

Synthesis of Room-Temperature Ionic Liquids with the Weakly Coordinating $[\text{Al}(\text{OR}^{\text{F}})_4]^-$ Anion ($\text{R}^{\text{F}} = \text{C}(\text{H})(\text{CF}_3)_2$) and the Determination of Their Principal Physical Properties

Safak Bulut,^[a] Petra Klose,^[a] Mian-Mian Huang,^[b] Hermann Weingärtner,^[b]
Paul J. Dyson,^[c] Gábor Laurenczy,^[c] Christian Friedrich,^[d] Jakob Menz,^[e]
Klaus Kümmerer,^[e] and Ingo Krossing*^[a]

Abstract: A large series of ionic liquids (ILs) based on the weakly coordinating alkoxyaluminate $[\text{Al}(\text{hfip})_4]^-$ (hfip: hexafluoroisopropoxy) with classical as well as functionalized cations were prepared, and their principal physical properties determined. Melting points are between 0 ($[\text{C}_4\text{MMIM}][\text{Al}(\text{hfip})_4]$) and 69 °C ($[\text{C}_3\text{MPip}][\text{Al}(\text{hfip})_4]$); three qualify as room-temperature ILs (RTILs). Crystal structures for six ILs were determined; their structural parameters and anion–cation contacts are compared here with known ILs, with a special focus on their influence on physical properties. Moreover, the biodegradability of the compounds was investigated by using the closed-bottle and the manometric respirometry test.

Temperature-dependent viscosities and conductivities were measured between 0 and 80 °C, and described by either the Vogel–Fulcher–Tammann (VFT) or the Arrhenius equations. Moreover, conductivities and viscosities were investigated in the context of the molecular volume, V_m . Physical property– V_m correlations were carried out for various temperatures, and the temperature dependence of the molecular volume was analyzed by using crystal structure data and DFT calculations. The IL ionicity was investigated by Walden plots;

according to this analysis, $[\text{Al}(\text{hfip})_4]^-$ ILs may be classified as “very good to good ILs”; while $[\text{C}_2\text{MIM}][\text{Al}(\text{hfip})_4]$ is a better IL than $[\text{C}_2\text{MIM}][\text{NTf}_2]$. The dielectric constants of ten $[\text{Al}(\text{hfip})_4]^-$ ILs were determined, and are unexpectedly high ($\epsilon_r = 11.5$ to 16.8). This could be rationalized by considering additional calculated dipole moments of the structures frozen in the solid state by DFT. The determination of hydrogen gas solubility in $[\text{Al}(\text{hfip})_4]^-$ RTILs by high-pressure NMR spectroscopy revealed very high hydrogen solubilities at 25 °C and 1 atm. These results indicate the significant potential of this class of ILs in manifold applications.

Keywords: conducting materials • dielectric constants • green chemistry • hydrogen • ionic liquids


[a] Dipl.-Chem. S. Bulut, P. Klose, Prof. Dr. I. Krossing
Albert-Ludwigs-Universität Freiburg
Institut für Anorganische und Allgemeine Chemie
and Freiburger Materialforschungszentrum (FMF)
Albertstr. 21, 79104 Freiburg (Germany)
E-mail: krossing@uni-freiburg.de

[b] M. Sc. M.-M. Huang, Prof. Dr. H. Weingärtner
Physical Chemistry 2, Ruhr-University Bochum
44780 Bochum (Germany)

[c] Prof. Dr. P. J. Dyson, Dr. G. Laurenczy
Institut des Sciences et Ingénierie Chimiques
École Polytechnique Fédérale de Lausanne (EPFL)
1015 Lausanne (Switzerland)

[d] Prof. Dr. C. Friedrich
Albert-Ludwigs-Universität Freiburg
Freiburger Materialforschungszentrum (FMF)
Stefan-Meier-Str. 21, 79104 Freiburg (Germany)

[e] J. Menz, Prof. Dr. K. Kümmerer
Leuphana University Lüneburg
Institute of Ecology and Environmental Chemistry
Scharnhorststr. 1, 21335 Lüneburg (Germany)

 Supporting information for this article is available on the WWW under <http://dx.doi.org/10.1002/chem.201000982>.

Introduction

Ionic liquids (ILs) are generally defined as salts with melting points (m.p.) below 100 °C; those that melt below 25 °C are termed room-temperature ionic liquids (RTILs). They are of interest for a multitude of applications; for example, as reaction media,^[1–2] as electrolytes in batteries and super capacitors,^[3–7] in solar and fuel cells,^[8–13] for electrochemical deposition of metals and semiconductors,^[14] as additives for stabilizing proteins,^[15] for liquid–liquid extractions,^[16] and in nanoscience.^[17–19] ILs are expected to play an important role in green and sustainable chemistry; the assessment of their biodegradability in sewage treatment or surface water is an important aspect in this context.^[20,21]

The physical properties of ILs are connected to many physical observables, in which the anion–cation interactions and the size of the ions as measured by the molecular volume V_m , for example, probably play the most important role.^[22,23] In general, one can expect that weaker anion–cation interactions lead to lower melting salts with lower viscosities and higher conductivities.^[22,24] The strength of these anion–cation interactions are correlated to some extent with the coordination ability and Lewis basicity of the anion.^[25] Thus, weakly coordinating anions (WCA) are good candidates for the synthesis of new salts with lower m.p.s and other optimized physical properties. It is well known that $[\text{Al}(\text{hfip})_4]^-$ (hfip: hexafluoroisopropoxy; $\text{OC}(\text{H})(\text{CF}_3)_2$) is a WCA that has been used in our group to stabilize reactive cations since 1999^[25–34] (see Figure 1). For the synthesis of

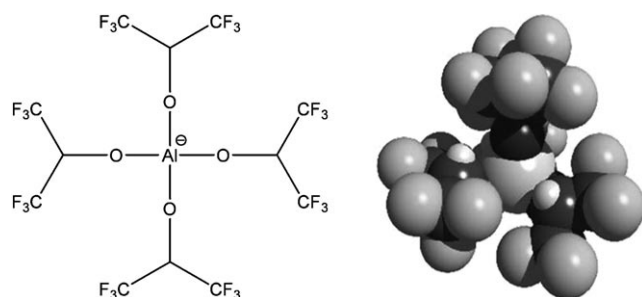


Figure 1. Schematic and space filling representation of the $[\text{Al}(\text{hfip})_4]^-$ WCA used in the synthesis of the new ILs in this work.

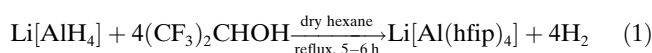
new compounds with $[\text{Al}(\text{hfip})_4]^-$ as an anion, $\text{Li}[\text{Al}(\text{hfip})_4]$, a colorless solid with a m.p. of 120 °C, is the usual starting material. If the Li^+ cation is exchanged for a typical weakly coordinating IL-type cation, one obtains $[\text{Al}(\text{hfip})_4]^-$ ILs as initially explored by Mudring et al. for two ILs with this anion type (m.p. 34 and 47 °C).^[35,36] Since the polyfluoroalkoxyaluminates have lower Lewis basicity and coordinating ability than conventional solvents, the use of $[\text{Al}(\text{hfip})_4]^-$ ILs as reaction media is a very interesting proposition. The high electrochemical stability of the anion is another advantage (>5.0 V versus Li/Li^+ ; used as electrolyte).^[37] ILs with $[\text{Al}(\text{hfip})_4]^-$ as the anion are thus of interest due to the high electrochemical stability of this anion as well as for the sta-

bilization of highly reactive, redox-active cations. In earlier work we observed relatively low melting temperatures of 42 to 61 °C for the symmetrical ammonium salts of this anion with various alkyl groups, which can already be categorized as ILs.^[38] With symmetrical ions the lattice energy is usually higher than with less symmetrical ions. Thus, we expected that even room-temperature ILs should be accessible by using less symmetrical cations than NR_4^+ .

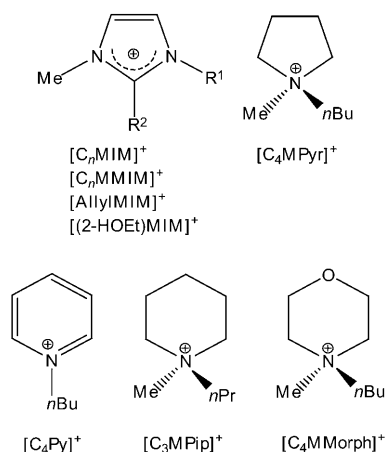
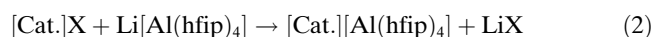
Because the starting materials used to prepare compounds of the fluorinated aluminates are commercially available (see e.g., <http://www.fluorine.ru>) and the synthesis of the lithium aluminate salt^[34,39–41] is a simple, high yielding procedure that we have performed in scales up to 250 g per batch,^[40] it appeared logical to extend the available ILs to further cation classes.

Results and Discussion

Synthesis and characterization: In the first step (reaction 1), $\text{Li}[\text{Al}(\text{hfip})_4]$ was synthesized by reacting pure $\text{Li}[\text{AlH}_4]$ and dry hexafluoroisopropanol in dry hexane, as shown in Equation (1):^[39]



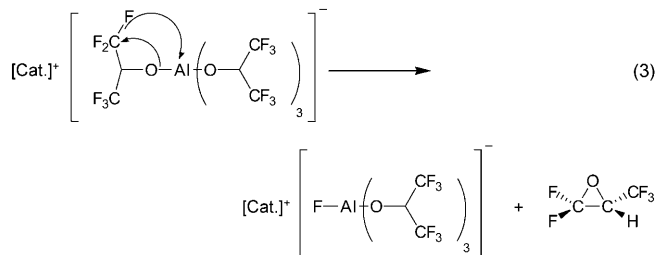
The reaction works very well with yields exceeding 95 % for the optimized procedure.^[40,41] In the anion metathesis reaction, lithium was exchanged for substituted imidazolium, pyrrolidinium, pyridinium, piperidinium, and morpholinium cations [see Scheme 1 and Eq. (2)]:



Scheme 1. Cations used in the reaction shown in Equation (2). $[\text{C}_n\text{MIM}]^+$ = 1-alkyl-3-methylimidazolium, in which n is the length of the alkyl chain. $[\text{C}_n\text{MMIM}]^+$ = 1-alkyl-2,3-dimethylimidazolium, in which n is the length of the alkyl chain. $[\text{AllyMIM}]^+$ = 1-allyl-3-methylimidazolium. $[(2\text{-HOEt})\text{MIM}]^+$ = 1-(2-hydroxyethyl)-3-methylimidazolium. $[\text{C}_4\text{MPyr}]^+$ = *N*-butyl-*N*-methylpyrrolidinium. $[\text{C}_4\text{Py}]^+$ = *N*-butylpyridinium. $[\text{C}_3\text{MPip}]^+$ = *N*-propyl-*N*-methylpiperidinium. $[\text{C}_4\text{MMorph}]^+$ = *N*-butyl-*N*-methylmorpholinium.

Anion metathesis took place in dry CH_2Cl_2 . The mixture was stirred at room temperature for 24 h and then filtered over siliceous earth (which was the best of all tested filter materials for eliminating the LiCl precipitate). Before filtration, the siliceous earth in the Schlenk frit was rinsed several times with dry CH_2Cl_2 and dried under vacuum for 3–4 h with heating at 350–500 °C. After filtration a clear solution was obtained. Because the $[\text{Al}(\text{hfp})_4]^-$ anion is water sensitive, the chloride/bromide content could not be determined by ion chromatography (IC); thus it was tested by using aqueous AgNO_3 solution, and did not show any indication of AgX formation. For the same reason, no Karl Fischer titration could be performed to determine the water content; however, great care was taken to ensure that all materials were free of residual water (procedures were carried out in a glove box with <1 ppm H_2O and O_2 , and by use of vacuum lines with vacuum of 0.1 Pa inside the flasks). After filtration, the solvent was removed by vacuum distillation. The remaining product was rinsed with dry hexane and dried under high vacuum (0.1 Pa) for one day until a constant weight was achieved. Typical yields of the purified product were 90 to 95 %.

Purity considerations: No traces of decomposition were observed in the ^1H , ^{27}Al NMR, and IR or Raman spectra. However, slight traces of decomposition were observed in some ^{19}F NMR spectra. All experimental spectra of the ILs used for further investigations can be found in the Supporting Information. To analyze this slight decomposition, several samples were examined by NMR spectroscopy during the reaction, and before and after the filtration over siliceous earth. The NMR spectra of the samples before and after the filtration over siliceous earth were identical, and showed absolutely no trace of decomposition in the ^{19}F NMR spectra. The decomposition visible in the ^{19}F NMR spectra of the pure ILs was only observed after the CH_2Cl_2 was removed and the IL was dried for several hours in vacuum (0.1 Pa). Thus, we can exclude the possibility that the decomposition was caused by water impurities or by the synthesis method. It is known from MS that the $[\text{Al}(\text{OR}^{\text{F}})_4]^-$ anions ($\text{R}^{\text{F}} = \text{C}(\text{CF}_3)_3$, $\text{C}(\text{CH}_3)(\text{CF}_3)_2$, or $\text{CH}(\text{CF}_3)_2$) decompose in the ion trap of the MS with evolution of $[\text{F}-\text{Al}(\text{OR}^{\text{F}})_3]^-$ and the appropriate epoxide, as shown in Equation (3).^[38]



Related fluorinated epoxides are known^[42–44] and are very volatile. It appears that the epoxide is immediately removed during vacuum drying and in the ^{19}F NMR spectra only a small additional signal of the decomposed $[\text{F}-\text{Al}(\text{OR}^{\text{F}})_3]^-$

anion is visible. We investigated one of the samples by mass spectrometry and detected by NMR spectroscopy the expected signals of the main and decomposition products $[\text{Al}(\text{hfp})_4]^-$ (m/z 695) and $[\text{F}-\text{Al}(\text{hfp})_3]^-$ (m/z 547) anions in a 100:7.3 ratio. The amount of $[\text{F}-\text{Al}(\text{hfp})_3]^-$, as determined by ^{19}F NMR spectroscopy, was 3.3 % in **1**, 4.5 % in **2**, 1 % in **4**, 2.3 % in **6**, 1 % in **7**, 1 % in **9**, and 4.4 % in **10**. No decomposition was observed for **3**, **5**, or **8**. However, prolonged heating under vacuum should be avoided with these $[\text{Al}(\text{hfp})_4]^-$ ILs. It should be noted that the metathesis with (2-HOEt)MIM $^+X^-$ presented problems; rather erratically, it produced very viscous materials that were either pure according to the NMR spectroscopy or considerably contaminated. Therefore, we did not include data for this IL in the following.

Melting points (T_m) of $[\text{Cat}][\text{Al}(\text{hfp})_4]$: Melting points (T_m) were determined from differential scanning calorimetry (DSC) experiments run on a SETARAM DSC 131 instrument; to infer the melting temperatures, the onset points have been taken into account (heating rate 5 K min^{-1}).

The melting points of the salts are between 0 (**8**) and 69 °C (**6**) and the salts can thus be categorized as ILs; three were under 25 °C, which qualifies the salts as RTILs. Mudring et al. found similar melting temperatures for the previously reported salts, **5** and **7** (see Table 1),^[35] which suggests that the melting temperatures found here are reproducible.

Table 1. Melting points T_m and crystallization temperatures T_c of the $[\text{Al}(\text{hfp})_4]^-$ ILs investigated in this study.

Salt	T_m [°C]	T_c [°C]
$[\text{C}_2\text{MIM}][\text{Al}(\text{hfp})_4]$ (1)	31	$<25^{\text{[a]}}$
$[\text{AllylMIM}][\text{Al}(\text{hfp})_4]$ (2)	12	–24
$[\text{C}_2\text{MMIM}][\text{Al}(\text{hfp})_4]$ (3)	39	34
$[\text{C}_4\text{Py}][\text{Al}(\text{hfp})_4]$ (4)	36	$<25^{\text{[a]}}$
$[\text{C}_4\text{MIM}][\text{Al}(\text{hfp})_4]$ (5)	40 ^[b]	$<25^{\text{[a,b]}}$
$[\text{C}_3\text{MPip}][\text{Al}(\text{hfp})_4]$ (6)	69	58
$[\text{C}_4\text{MPyr}][\text{Al}(\text{hfp})_4]$ (7)	50 ^[b]	39 ^[b]
$[\text{C}_4\text{MMIM}][\text{Al}(\text{hfp})_4]$ (8)	0	–35
$[\text{C}_4\text{MMorph}][\text{Al}(\text{hfp})_4]$ (9)	31	6
$[\text{C}_6\text{MIM}][\text{Al}(\text{hfp})_4]$ (10)	5	–5

[a] No crystallization peak was observed in the working temperature ranges (measurements were carried out starting from RT for these ILs). [b] Reported melting (crystallization) temperatures for **5** and **7** are +34 (–19) and +47 (+21) °C, respectively.^[35]

Thermal stability by DSC: It was reported that the thermal decomposition of the symmetrical ammonium salts of the $[\text{Al}(\text{hfp})_4]^-$ anion started above 150 °C.^[38] The ILs studied in this work were heated to 150–250 °C during DSC investigations. From the DSC traces, no clear single decomposition pathway could be identified; as shown, for example, in Figure 2a) for **6**. However, clear decomposition signals for **7** were observed at 155, 183, and 261 °C (see Figure 2b)). Following decomposition, only very small residual crystallization and melting signals were visible. Similarly, the decomposition of **9** was observed at 164 and 235 °C, and of **3** at 172–176 °C.

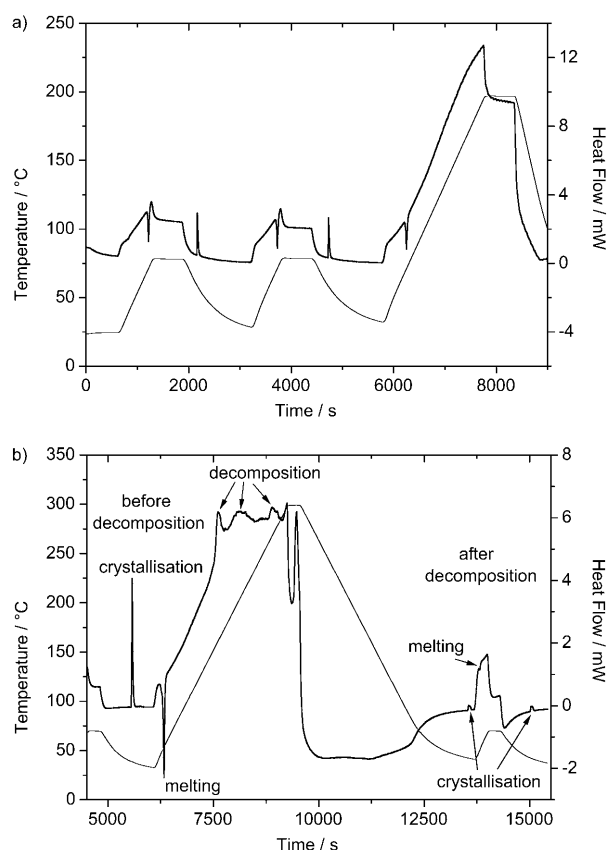


Figure 2. a) DSC traces of **6**. No clear single decomposition pathway is identifiable. b) Decomposition of **7** by DSC. The decompositions were observed at 155, 183 and 261 °C (the onset points have been taken into account). —: temperature, — —: heat flow.

From these measurements it follows that thermal decomposition of $[\text{Al}(\text{hfp})_4]^-$ -based ILs with various types of cations begins around 150 °C.

Biodegradability: The biodegradability of four $[\text{Al}(\text{hfp})_4]^-$ ILs (**2**, **8**, **9**, **10**) was investigated in the closed bottle test (CBT) and the manometric respirometry test (MRT). Full details are given in the Supporting Information.

Biodegradability in the CBT: The CBT proved to be valid, because in both quality controls the readily degradable sodium acetate was eliminated by at least 60% within 14 days. None of the test compounds showed any aerobic biodegradation, as shown in Figure S4 in the Supporting Information for **9**. No toxicity against bacteria was shown in the toxicity control vessels.

Biodegradability in the MRT: In the MRT comparable results were found for the four test compounds. Neither aerobic degradation nor toxicity to bacteria in the toxicity controls could be observed as shown in Figure S5 in the Supporting Information for **2**. The readily degradable sodium acetate was eliminated by approximately 80% within 14 days, which confirms the validity of the test.

Thus, MRT and CBT suggest that none of the four investigated ILs bearing fluorinated aluminate anions could be classified as “readily biodegradable”.

Solid-state structures: Crystals suitable for X-ray diffraction were obtained for **1**, **2**, **3**, **4**, **6**, and **9** (see Table 11 in the Experimental Section for crystallographic details). The diffraction measurements were carried out at 100 to 120 K to minimize rotation of the CF_3 groups. In Table 2, the most characteristic structural parameters of the anion (the Al–O lengths and the O–Al–O and Al–O–C bond angles) are listed. A short description of the packing patterns is also given in Table 2; packing diagrams of all compounds are provided in the Supporting Information. Since the anions are larger than the cations, their packing is described based on the anion lattice.

Table 2. Structural information of the $[\text{Al}(\text{hfp})_4]^-$ salts with various cations at 100–120 K.

	1	2	3	4	6	9
$d(\text{Al–O})$ range [pm]	173.0(7)– 175.1(6)	173.21(11)– 174.64(11)	173.54(18)– 174.31(18)	173.6(3)– 174.5(3)	173.1(4)– 175.3(3)	172.80(17)– 174.16(17)
$d(\text{Al–O})$ average [pm]	174.05	173.83	173.97	173.95	173.80	173.69
$\angle(\text{O–Al–O})$ range [°]	107.7(3)– 111.6(3)	107.26(6)– 112.46(6)	104.64(9)– 116.99(9)	107.48(14)– 111.88(14)	108.21(17)– 111.43(17)	106.99(8)– 113.11(9)
$\angle(\text{Al–O–C})$ range [°]	126.7(5)– 130.8(7)	127.23(9)– 131.95(10)	127.42(15)– 132.34(16)	128.3(2)– 131.8(2)	125.5(3)– 131.3(3)	127.33(16)– 134.10(16)
$\angle(\text{Al–O–C})$ average [°]	129.1	129.4	129.2	129.6	128.1	130.6
$V_{\text{cation}}/V_{\text{anion}}^{[a]}$	0.292	0.322	0.315	0.319	0.395	0.418
$r_{\text{cation}}/r_{\text{anion}}^{[b]}$	0.663	0.685	0.680	0.683	0.734	0.748
packing	distorted NaCl	distorted NaCl	distorted NaCl	distorted NaCl	distorted CsCl	distorted CsCl
shortest contacts [pm]	228.5 (H...O)	227.2 (H...O)	247.0 (H...O)	250.1 (H...F)	246.2 (H...F)	245.2 (H...F)
($A_{\text{cation}} \dots B_{\text{anion}}$) ^[c]	252.6 (H...F)	246.5 (H...F)	257.3 (H...F)	250.7 (H...F)	246.8 (H...F)	248.8 (O...H)
dipole moment A^- [D] ^[d]	2.38	2.99	0.54	2.95	3.25	3.72
dipole moment C^+ [D] ^[d]	1.66	3.25	1.47	3.32	0.89	2.19
dipole moment C^+A^- [D] ^[d]	18.35	31.3	25.4	19.23	25.01	38.98

[a] The cation volume was calculated by using the cell volume for each salt and subtracting the anion volume.^[38] [b] The ratio of the radii has been calculated from the volume/volume ratio assuming that the ions are spherical, $r_{\text{cation}}/r_{\text{anion}} = (V_{\text{cation}}/V_{\text{anion}})^{1/3}$. [c] Secondary contacts $\angle \Sigma$ van der Waals radii. [d] Dipole moments in debye are taken from single-point DFT calculations at the BP86/SV(P) level starting with crystal structure coordinates of the anion (A^-), the cation (C^+), and the ion pair (C^+A^-) from the asymmetric unit.

As can be seen from the structural parameters of the anion listed in Table 2, the Al atoms are in close to ideal tetrahedral environments. The bond lengths and angles in the anion for the various salts are similar to each other, and are also in a good agreement with other reported salts of the anion.^[35,38,39,45] The ion packing of the four ILs **1** to **4** is best described as distorted NaCl-type packing, whereas for **6** and **9** a distorted CsCl packing was observed, which was indeed expected according to the radii ratio rule (salts with $r_{\text{cation}}/r_{\text{anion}} > 0.414$ show NaCl-type packing; salts with $r_{\text{cation}}/r_{\text{anion}} > 0.732$ show CsCl-type packing).^[46] In Table 3, the shortest secondary contacts below the sum of the van der Waals radii in ILs with various anions are compared with those of the [Al(hfip)₄]⁻ anion. Note that almost all contacts in the [Al(hfip)₄]⁻ ILs are longer than those in other comparable ILs with the same cation.

Table 3. Comparison of the two shortest contacts in the ILs with different anion types (ILs of the same cation types, with the same or similar alkyl chains). All contacts (A · · · B) refer to atom A from the cation and atom B from the anion. [C_nPy]⁺ = N-alkylpyridinium, [TfO]⁻ = trifluoromethanesulfonate, [Tf₂N]⁻ = bis(trifluoromethylsulfonyl) imide, for other abbreviations see Scheme 1.

IL	Shortest contact [pm]	Next shortest contact [pm]
[C ₂ MIM][BF ₄] ^[47]	227.1 (H··F)	237.9 (H··F)
[C ₂ MIM][PF ₆] ^[48]	249.0 (H··F)	253.6 (H··F)
[C ₂ MIM][AsF ₆] ^[49]	254.3 (H··F)	259.2 (H··F)
[C ₂ MIM][TfO] ^[50]	224.4 (H··O)	237.1 (H··O)
[C ₂ MIM][Tf ₂ N] ^[51]	225.4 (H··O)	247.4 (H··O)
[C ₂ MIM][Al(hfip) ₄] (1)	228.5 (H··O)	252.6 (H··F)
[C ₁ MMIM][TfO] ^[52]	242.4 (H··O)	242.9 (H··O)
[C ₂ MMIM][Al(hfip) ₄] (3)	247.0 (H··O)	257.3 (H··F)
[C ₆ Py][Tf ₂ N] ^[47]	230.9 (H··O)	244.9 (H··O)
[C ₄ Py][Al(hfip) ₄] (4)	250.1 (H··F)	250.7 (H··F)

Viscosities and conductivities: The results of the temperature-dependent viscosity and conductivity measurements are given in Table 4. The viscosity measurements were performed as a function of speed and torque. All of these [Al(hfip)₄]⁻ ILs are Newtonian fluids (the viscosity is independent of speed and torque, tested in the torque range from 5 to 98%). The viscosity of some ILs could be measured at

Table 4. Temperature-dependent viscosities (η) of the [Al(hfip)₄]⁻ ILs and their molecular volumes (V_m).

[Al(hfip) ₄] ⁻ ILs	V_m [nm ³]	η [cP]									
		0 °C	10 °C	20 °C	25 °C	30 °C	40 °C	50 °C	60 °C	70 °C	80 °C
1	0.731	–	–	–	–	–	24.4	18.2	13.4	10.3	8.2
2	0.749	–	–	46.1	37.7	–	22.4	17.3	12.7	9.5	8.2
3	0.755	–	–	–	–	–	–	21.5	15.8	11.9	9.3
4	0.774	–	–	–	–	37.9	25.1	17.7	13.1	10.0	7.9
5	0.779	–	–	–	–	–	21.8	15.8	11.7	9.0	7.1
7	0.795	–	–	–	–	–	–	–	16.7	13.1	10.2
8	0.800	155.5	86.8	52.1	42.0	34.4	23.6	16.9	12.5	9.6	7.7
9	0.804	–	–	–	86.6	70.4	41.3	27.3	17.9	12.4	9.1
10	0.826	166.2	90.7	54.4	43.5	35.4	25.3	18.2	13.2	10.1	7.8
11	0.973	–	–	–	–	–	49.9	31.7	21.6	15.1	11.6

temperatures lower than their melting points, because their freezing points were often 5 to 35 °C below the melting temperatures (see Table 1). The conductivities of the ILs were measured between 22.5–80 °C (Table 5) with a Metrohm 712 conductometer in an argon-filled glove box (water and oxygen content < 1 ppm). Their temperatures were measured with a metal thermostat (accuracy ca. ± 0.1 °C, see photo in the Supporting Information). The viscosity and conductivity of **6** could not be measured due to its high melting point of 69 °C.

Description of the temperature dependence of the viscosity and conductivity

Viscosity: Arrhenius-type behavior has been widely used to describe the temperature dependence of the viscosity of liquids. However, VanderNoot et al. measured the absolute viscosity of 23 RTILs as a function of the temperature; they found that the Arrhenius plot is not linear for the majority of the RTILs; some fit better with the Vogel–Fulcher–Tammann (VFT) equation.^[53] Brennecke et al. determined the viscosity for binary mixtures of water and three ionic liquids. They found that the temperature dependence of viscosity for these systems could be described by an empirical second-order polynomial, and by the VFT equation.^[54] Equation (4) is the VFT equation used to describe the temperature dependence of the viscosity for [Al(hfip)₄]⁻ ILs:

$$\eta = (A_\eta \sqrt{T}) e^{k_\eta / (T - T_0)} \quad (4)$$

T_0 is often described as the ideal glass transition temperature (corresponds to the temperature at which the viscosity is infinite), k_η is a constant, the product $k_\eta R$ has been related to the Arrhenius activation energy, and A_η is another constant.^[55,56]

The temperature dependency of the viscosity was described for eleven [Al(hfip)₄]⁻ ILs by using the VFT equation with very good regressions for all plots ($R^2 \geq 0.99$), as shown in Figure 3. The constants A_η , k_η , and T_0 were determined from the VFT fit (Table 6). For some ILs high errors by VFT parameters were observed due to there being few viscosity data points available for these ILs. In general, as many data points were used as possible for the VFT fit. Additional data points to those given in Table 4 were also recorded at 15, 35, 45, 55, 65, and 75 °C (if compatible with the liquid range of the IL in question).

Conductivity: In contrast to viscosity, the Arrhenius equation [Eq. (5)] is often used, because it is more suitable for describing the temperature depend-

Table 5. Temperature-dependent conductivities (σ) of the $[\text{Al}(\text{hfiip})_4]^-$ ILs and their molecular volumes (V_m).

$[\text{Al}(\text{hfiip})_4]^-$ ILs	V_m [nm ³]	22.5 °C	25 °C	30 °C	35 °C	40 °C	50 °C	60 °C	70 °C	80 °C
1	0.731	–	–	–	–	6.22	6.88	8.63	10.91	11.01
2	0.749	3.78	4.24	5.36	6.09	6.86	8.46	11.48	13.27	15.05
3	0.755	–	–	–	–	–	4.68	6.77	9.32	11.71
4	0.774	–	–	–	–	–	–	–	10.22	12.74
5	0.779	–	–	–	–	–	5.71	7.19	9.57	10.51
7	0.795	–	–	–	–	–	–	–	7.15	9.12
8	0.800	2.34	2.53	2.96	3.46	4.08	4.65	6.68	8.81	10.35
9	0.804	–	–	–	–	1.99	2.68	3.67	5.25	6.78
10	0.826	2.13	2.36	2.72	3.25	3.57	4.57	6.35	8.12	10.14
11	0.973	–	–	–	–	–	1.66	2.27	2.96	3.74

in which A is the conductivity at infinite temperature, E_a is the activation energy, and R is the universal gas constant. By fitting the conductivity against the reciprocal temperature a very good fit for $[\text{Al}(\text{hfiip})_4]^-$ ILs was observed ($R^2 \geq 0.95$), as shown in Figure 4. Thus, the temperature dependency of the conductivity for $[\text{Al}(\text{hfiip})_4]^-$ ILs in the temperature range of 22.5–80 °C can be described as Arrhenius-type behavior. A and E_a are included in Table 6.

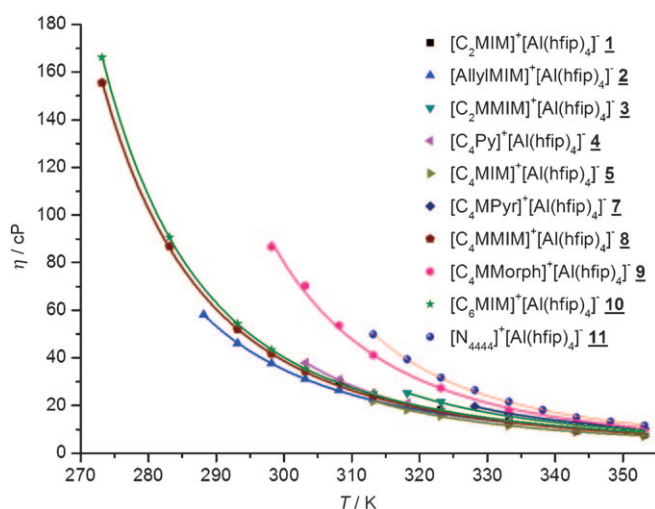


Figure 3. The temperature dependence of the viscosity (η) for $[\text{Al}(\text{hfiip})_4]^-$ ILs: Experimental values are indicated by symbols and the line is fit by the VFT relation [Eq. (4)].

Table 6. Parameters for the $[\text{Al}(\text{hfiip})_4]^-$ ILs in the VFT equation [Eq. (4)], determined from the VFT fits in Figure 3 (columns 2–4); and in the Arrhenius equation [Eq. (5)], determined from the Arrhenius fits in Figure 4 (columns 5–6).

IL	A_η [cP K ^{-0.5}]	k_η [K]	T_0 [K]	A [mS cm ⁻¹]	E_a/R [K]
1	0.0164 ± 0.0153	522.9 ± 234.7	195.4 ± 27.9	1780.3	1777.4
2	0.0139 ± 0.0059	618.7 ± 106.8	175.8 ± 10.8	19298	2498.7
3	0.0226 ± 0.0294	438.7 ± 302.8	212.3 ± 39.6	250834.2	3511.3
4	0.0152 ± 0.0052	513.6 ± 78.1	199.8 ± 8.6	–	–
5	0.0181 ± 0.0129	449.5 ± 168.6	206.9 ± 21.8	10502.7	2424.6
7	0.0657 ± 0.0936	222.2 ± 249.4	248.9 ± 47.7	–	–
8	0.0075 ± 0.0019	758.9 ± 59.2	166.9 ± 4.6	23476.2	2723.5
9	0.0049 ± 0.0093	818 ± 491	180.7 ± 38.3	121601.8	3458.5
10	0.0103 ± 0.0022	684.5 ± 47.6	173.8 ± 3.8	29298.1	2815.6
11	0.0165 ± 0.0088	499.2 ± 114.7	216.1 ± 12.1	23260	3079.7

ence of the conductivity; Equation (5) contains two parameters, and the temperature is only included with the exponential term,

$$\sigma = Ae^{-E_a/RT} \quad (5)$$

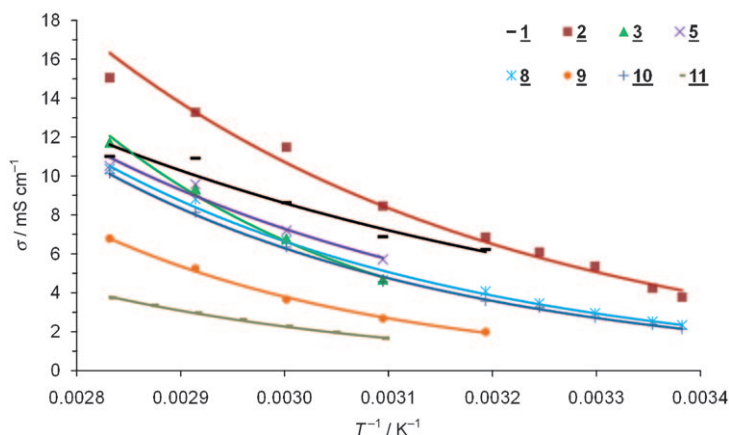


Figure 4. Description of the temperature dependence of the conductivity (σ) for $[\text{Al}(\text{hfiip})_4]^-$ ILs by using the Equation (5). The data of the salts **4** and **7** were not fitted because only very few data points were available.

Correlations between physical properties and molecular volume (V_m):

In earlier work, we reported the correlation between molecular volume and physical properties; for example, viscosities, conductivities, densities, and heat capacities (C_p) of ILs.^[23,24] Very good correlations were observed in these studies by using classical, nonfunctionalized ILs. These correlations allow the prediction of the physical properties of new, unknown salts. Because an enormous number of salts have the potential to form ILs (it has been estimated that there may be up to 10^{12} – 10^{18} ILs^[57,58]) the prediction of the physical properties of unknown ILs is of importance.

The molecular volume (V_m) is a physical observable, and is defined as the sum of the ionic volumes of the constituent ions (V_{ion}), which can be determined from X-ray crystal structures. V_{ion} can be determined from a crystal structure containing one of the ions of interest in combination with a reference ion for which the ion volume has been previously established^[22,24] (many of such reference ions can be found in large databases, including the CCDC database^[59] and others^[60,61]). A disadvantage of the experimentally determined ionic volumes is the possible inaccuracies that may arise because the temperatures at which the structure deter-

minations were performed are completely neglected. Only ion volumes determined at the same temperature can be compared with each other. Unfortunately, all literature data have neglected this fact. Recently, we reported a new method to calculate the molecular volume V_m by using quantum chemical calculations and correlations of calculated and experimental V_m values.^[23] The calculated V_m is independent of temperature and is thus internally consistent if used throughout an investigation—in contrast to the experimentally determined V_m . The best published method uses DFT structure calculations with the TURBOMOLE^[62] program package used with the resolution of identity^[63] (RI) approximation, and correlation of the calculated ionic volumes with experimentally determined ionic volumes.^[23] In Table 7 all ionic volumes used in this work are shown. These

Table 7. Scaled calculated ionic volumes (V_{ion}) of the ions investigated in this study (scaled BP86/TZVP/COSMO).^[23]

Ion	$V_{\text{ion}} [\text{nm}^3]$	Ion	$V_{\text{ion}} [\text{nm}^3]$
$[\text{C}_2\text{MIM}]^+$	0.149	$[\text{C}_4\text{MPyr}]^+$	0.213
$[\text{AllylMIM}]^+$	0.167	$[\text{C}_4\text{MMIM}]^+$	0.218
$[\text{C}_2\text{MMIM}]^+$	0.173	$[\text{C}_6\text{MMorph}]^+$	0.222
$[\text{C}_4\text{Py}]^+$	0.192	$[\text{C}_6\text{MIM}]^+$	0.244
$[\text{C}_4\text{MIM}]^+$	0.197	$[\text{N}_{444}]^+$	0.391
$[\text{C}_3\text{MPip}]^+$	0.209	$[\text{Al}(\text{hfip})_4]^-$	0.582

volumes were obtained from gas-phase structure optimizations, and were carried out by the BP86/TZVP^[64] method, followed by COSMO^[65] calculations with TURBOMOLE.^[62]

In Table 8 the molecular volumes of some $[\text{Al}(\text{hfip})_4]^-$ ILs determined from their crystal structures at various temperatures are shown. The ionic volumes were calculated by subtracting the counter-ion volumes from these experimentally determined molecular volumes. We focus here on the volume of the $[\text{Al}(\text{hfip})_4]^-$ anion, for which we calculated a scaled molecular volume of 0.582 nm^3 ((RI)-BP86/TZVP^[23]).

Table 8 shows that the anion volumes, obtained by subtraction of the temperature-independent scaled calculated cation volumes from the experimental V_m , range from 0.569 to 0.610 nm^3 . They show a clear dependence on temperature, with higher temperatures leading to larger volumes (as expected when one considers thermal expansion of the unit cell on warming). Despite varying cation types, the anion volumes remain very similar for similar measurement temperatures; for example, the anion volumes obtained from the 113 K crystal structures of $[\text{C}_2\text{MIM}]^+$, $[\text{C}_3\text{MPip}]^+$, and $[\text{C}_4\text{MMorph}]^+$ are the same within error limits (0.596 to 0.597 nm^3).

When comparing cation volumes, we also observe various volume changes for a CH_2 group. The difference in volume change from $[\text{C}_2\text{MIM}]^+$ to $[\text{C}_2\text{MMIM}]^+$ is 0.013 nm^3 , but in going from $[\text{C}_2\text{MMIM}]^+$ to $[\text{C}_4\text{MIM}]^+$ it increases by 0.048 nm^3 . The volumes of the cations can also be compared with reported values (see last column in Table 8), which shows differences of up to 0.029 nm^3 . Analysis of the data

Table 8. Molecular volumes (V_m) determined experimentally (X-ray) at given temperatures of the $[\text{Al}(\text{hfip})_4]^-$ ILs and the corresponding ion volumes.

IL	$V_{m,\text{calcd}}^{\text{[a]}}$ [nm^3]	T [K] ^[b]	$V_{m,\text{exptl}}^{\text{[c]}}$ [nm^3]	$V^+_{\text{ion}}^{\text{[d]}}$ [nm^3]	$V^-_{\text{ion}}^{\text{[d]}}$ [nm^3]	$V^+_{\text{ion}}^{\text{[e]}}$ [nm^3]
1	0.731	113(2)	0.746	0.164	0.597	$0.156^{\text{[24]}}$
2	0.749	100(2)	0.763	0.181	0.596	–
3	0.755	120(2)	0.759	0.177	0.586	–
4	0.774	113(2)	0.761	0.179	0.569	$0.198^{\text{[24]}}$
5	0.779	173(2)	$0.807^{\text{[55]}}$	0.225	0.610	$0.196^{\text{[24]}}$
6	0.791	113(2)	0.805	0.223	0.596	–
9	0.804	113(2)	0.818	0.236	0.596	–
$[\text{N}_{1111}][\text{Al}(\text{hfip})_4]^-$	0.695	100(2)	$0.696^{\text{[58]}}$	0.114	0.583	$0.113^{\text{[60]}}$
$[\text{N}_{2222}][\text{Al}(\text{hfip})_4]^-$	0.782	150(2)	$0.805^{\text{[58]}}$	0.223	0.606	$0.232^{\text{[60]}}$

[a] $V_{m,\text{calcd}}$ is the calculated molecular volume; it corresponds to the sum of the scaled calculated ionic volumes of the constituent ions. The calculations are carried out as described in the text (DFT calculations with (RI-) BP86/TZVP method, followed by COSMO calculations with TURBOMOLE^[23]). [b] Temperatures of the crystal structure determinations. [c] $V_{m,\text{exptl}}$ is the experimental molecular volume; it corresponds to the sum of the ionic volumes of the constituent ions, here won from the crystal structure of each IL by dividing the unit cell volume (V_{cell}) by the number of the formula units per unit cell (Z). [d] The ionic volumes (V^+ and V^-) were obtained from $V_{m,\text{exptl}}$ by subtracting the counter-ion volume. As counter-ion volumes, the volumes received from DFT calculations were used as described above (Table 7; the volume of the ammonium cations, $[\text{N}_{1111}]^+$ and $[\text{N}_{2222}]^+$ is 0.113 and 0.199 nm^3 , respectively^[23]), in order to allow for a consistent comparison. [e] Cation volumes reported in the literature as determined from crystal structure data.

collected in Table 8 suggests that the experimental volumes of the various ions are preferable to use, as long as they were all determined at the same temperature. However, because it is often very difficult to find the data needed at the investigated temperatures, as shown in Table 8, an error is likely to be introduced when using the experimental values determined at different temperatures. Thus, for the correlations in this work, we always used calculated volumes, which were assessed with the same method for all ions, and which agree well with experimental volumes at an arbitrary, not assigned, average temperature.^[23]

By using the calculated molecular volumes, V_m (sum of the corresponding ionic volumes from Table 7) and viscosities in Table 4 or conductivities in Table 5, we can make correlations at various temperatures. Selected examples are shown in Figure 5 (a full account is provided in the Supporting Information).

As seen in Tables 4 and 5, the viscosities and conductivities change with the size of the salts (V_m) and temperature, as expected (with the exception of the functionalized salt **9**). The viscosities rise with increasing size (V_m) and decrease with increasing temperature (the reverse for conductivities). These trends are clearly seen in Figure 5, which shows that the slopes for all viscosity correlations are positive, and for all conductivity correlations are negative. For the functionalized morpholinium IL **9** higher viscosities and lower conductivities, in spite of its similar size (V_m) to other salts, were observed and, hence, in Figure 5 this salt is omitted. We assume that the additional oxygen donor atom in the cation

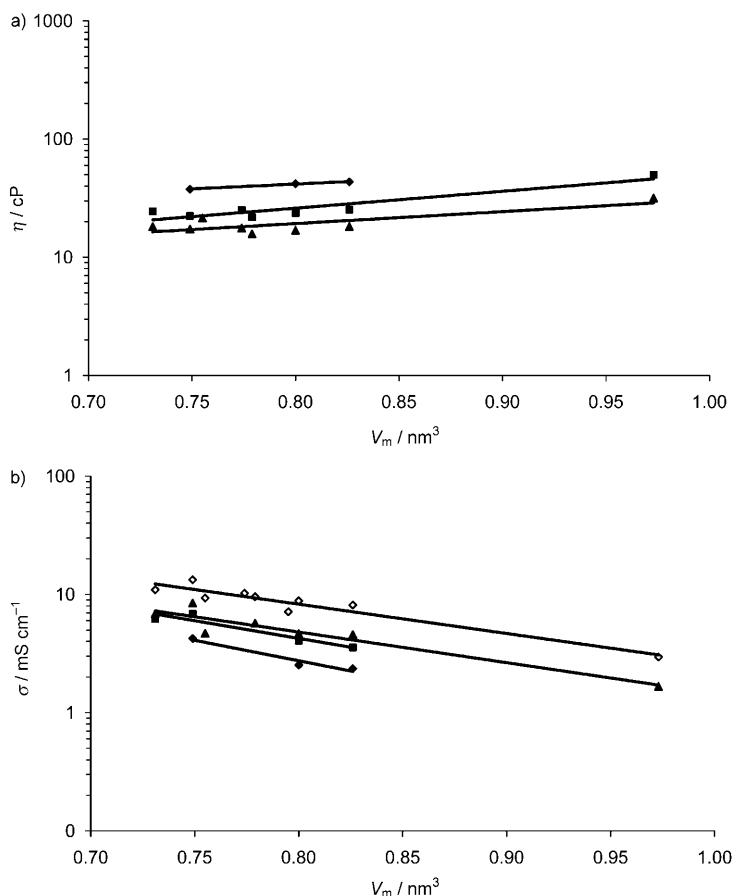


Figure 5. a) Correlation between molecular volume and viscosity by using the data from Table 4 at \blacklozenge 25 ($y=9.1099e^{1.8992x}$, $R^2=0.9911$), \blacksquare 40 ($y=1.8713e^{3.2895x}$, $R^2=0.8575$), and \blacktriangle 50 °C ($y=2.9879e^{2.3292x}$, $R^2=0.6507$). b) Correlation between molecular volume and conductivity by using the data from Table 5 at \blacklozenge 25 ($y=1598.5e^{-7.9575x}$, $R^2=0.9483$), \blacksquare 40 ($y=1042.6e^{-6.879x}$, $R^2=0.9109$), \blacktriangle 50 ($y=567.06e^{-5.9632x}$, $R^2=0.8925$), and \diamond 70 °C ($y=792.71e^{-5.7039x}$, $R^2=0.9157$). The axis of the viscosity and conductivity is scaled logarithmically.

structure leads to stronger contacts with the anion, which induce higher viscosity and lower conductivity (see discussion of the solid-state contacts below).

In our previous work on anion-dependent correlations between physical properties and molecular volume (V_m) of ILs, we observed that the slope of the correlation lines (the absolute value of the constant in the exponential term) is connected with the coordinative strength of the anion.^[24] The higher the coordination ability of the anion, the steeper the slope of the regression line, and thus the higher the absolute magnitude of the constant in the exponential term. It was observed that the slope slowly decreases from $[\text{BF}_4]^-/[\text{PF}_6]^-$ anions to $[\text{N}(\text{CN})_2]^-$ and $[\text{Tf}_2\text{N}]^-$ anions; probably due to the decreasing coordination ability of the anions in this order.^[24] Figure 6 shows anion-dependent correlations (molecular volume, viscosity, and conductivity at room temperature) for ILs based on the $[\text{Al}(\text{hfp})_4]^-$ anion in combination with other known anions ($[\text{BF}_4]^-/[\text{PF}_6]^-$, $[\text{N}(\text{CN})_2]^-$, and $[\text{Tf}_2\text{N}]^-$).

As expected, the absolute magnitude of the slope of the regression lines for the $[\text{Al}(\text{hfp})_4]^-$ ILs is lower. The magnitude of the constant in the exponential term decreases rapidly. The viscosity at 50 °C and higher temperatures is nearly independent of the cation (only nonfunctionalized cations) and the cation size plays almost no role. This is attributed to the nature of the WCA with a large fluorinated surface; the $[\text{Al}(\text{hfp})_4]^-$ anion leads to a minor dependence of viscosity and conductivity on the cation size and, generally, to ILs with low viscosities and high conductivities (compared with ILs based on smaller anions such as $[\text{Tf}_2\text{N}]^-$). This means that one may, in part, separate viscosities and conductivities from the cation type employed, due to the weak coordination ability of the $[\text{Al}(\text{hfp})_4]^-$ anion, which arises from its large fluorinated surface and very good negative charge distribution.

In Figure 7 the shortest anion–cation contacts of the functionalized morpholinium IL **9** are shown. The shortest contact was observed at 245.2 pm (H...F contact). This is similar to other cation types, in which shorter H...F and H...O contacts (H from cation, F and O from anion) were observed (see Table 2). However, the second shortest contact in **9** is an O...H contact at 248.8 pm, in which the basic O stems from the cation and the acidic H from the anion. This type of contact differentiates this functionalized IL from the other nonfunctionalized and structurally characterized $[\text{Al}(\text{hfp})_4]^-$ ILs; in all other structures reported here, the donor atoms (F, O) belong to the anion and the hydrogen acceptor atoms to the cation (Table 2). Thus, these contacts represent a typical donor–acceptor interaction, in which the anion A^- plays the role of the donor, and the cation C^+ the role of the acceptor ($\text{A}^- \rightarrow \text{C}^+$). But in the morpholinium IL **9** we also observed this effect in the other direction ($\text{C}^+ \rightarrow \text{A}^-$). The short ($\text{C}^+ \rightarrow \text{A}^-$) O...H contact shows that here the morpholinium cation with the oxygen atom at the ring also has a donor effect. Thus, there is electrostatic attraction in both directions, $\text{A}^- \leftrightarrow \text{C}^+$. This synergism probably causes a stronger cation–anion interaction, and is responsible for the stronger interaction in **9** than in nonfunctionalized salts, and thus leads to its different physical properties.

In Figure 8 the sigma surfaces of two cations, $[\text{C}_4\text{MMorph}]^+$ and the related $[\text{C}_3\text{MPip}]^+$ cation in which the ring oxygen is replaced by a CH_2 group, and the $[\text{Al}(\text{hfp})_4]^-$ anion are shown. The sigma surfaces were calculated with COSMO-RS^[66,67] by using coordinates optimized through DFT calculations in TURBOMOLE^[62] at the (RI)-BP86/TZVP^[64] level. The effect of the oxygen atom on the electron density distribution on the cation surface clearly emerges from these plots. The oxygen atom in the morpholinium ring is red, which indicates an increased negative charge relative to the nonfunctionalized piperidinium cation. Hence, this oxygen atom acts as a donor atom capable of forming additional contacts. The anion plot reveals that the position of the hydrogen atom is slightly positively charged, and the hydrogen atoms of the hexafluoroisopropoxy groups of the anion can act as acceptors.

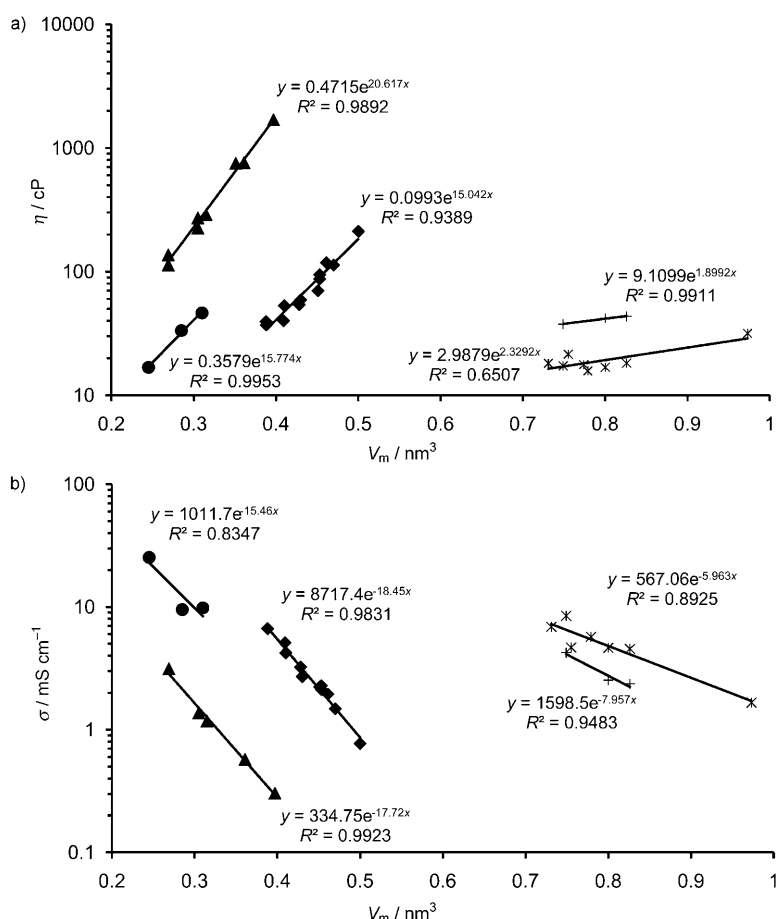


Figure 6. Correlations between a) molecular volume and viscosity and b) molecular volume and conductivity. \blacktriangle = $[\text{BF}_4]^-/[\text{PF}_6]^-$ salts, \bullet = $[\text{N}(\text{CN})_2]^-$ salts, \blacklozenge = $[\text{Tf}_2\text{N}]^-$ salts; all correlations for these salts are for data obtained at 20–22 °C.^[24] $+$ = $[\text{Al}(\text{hfp})_4]^-$ salts at 25 °C, $*$ = $[\text{Al}(\text{hfp})_4]^-$ salts at 50 °C. Viscosities and conductivities are plotted on logarithmic axes; x and y in the regression equations are V_m and η or σ , respectively.

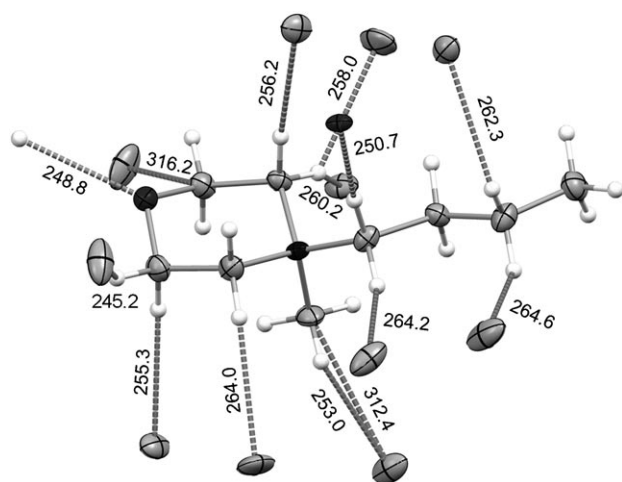


Figure 7. Section of the shorter anion–cation contacts (H...F, H...O, and C...F in pm) in the solid-state structure of **9** at 113(2) K. Thermal ellipsoids are drawn at the 25% probability level. The anion has been omitted for clarity. All contacts shown are shorter than the sum of the van der Waals radii (for H...F contacts 267 pm, for H...O contacts 272 pm, for C...F contacts 317 pm).

Walden product: Viscosity and conductivity are connected through the Stokes–Einstein and Nernst–Einstein equations. This connection produces the Walden rule,^[68,69] which states that the product of the viscosity and the molar conductivity is approximately constant.^[70,71] In recent years, work on the ionicity of ILs,^[72] liquid ion pairs,^[73] and protic ILs^[74–76] showed that the Walden rule is a useful way to assess the degree of the ionicity of ILs. This is done with the Walden plot. Yoshizawa and Angell et al. categorized ILs in conjunction with their ionicity, by using the Walden plot as the basis for a classification diagram, as super, good, poor etc.^[71] The logarithm of the molar conductivity (Λ_m) is plotted as a function of the logarithm of the fluidity (=inverse viscosity, η^{-1}). The Walden plot of a liquid yields an “ideal line” if all ions in the liquid are independent of each other. The ideal line corresponds to the situation in which the ions are moving individually in the absence of any ion–ion interactions, and the slope is approximately unity. A straight line that passes through the origin

and for which $\log(\Lambda_m) = \log(\eta^{-1})$ applies, was suggested as the ideal line. The position of the ideal line was established by using aqueous KCl solutions at high dilutions.^[71] In Figure 9 the Walden plots of the $[\text{Al}(\text{hfp})_4]^-$ -based ILs are shown. The viscosities and conductivities from Table 4 and Table 5 are plotted at various temperatures for each IL. The molar conductivity was obtained from the measured conductivity (in mS cm^{-1}) by using the molar mass and the density of the IL. The temperature-dependent densities required here were calculated according to previously published methods.^[23]

As seen from Figure 9, the Walden plots for all ILs lie less than an order of magnitude below the ideal line, and some of the $[\text{Al}(\text{hfp})_4]^-$ ILs are better than the $[\text{C}_2\text{MIM}][\text{Tf}_2\text{N}]$ reference IL determined in our labs. Hence all of these ILs qualify as at least “good” ILs.^[70,71,75] The reference $[\text{C}_2\text{MIM}][\text{Tf}_2\text{N}]$ is known as a good IL probably because of its weak anion–cation interactions and hence more ionic constitution.^[72]

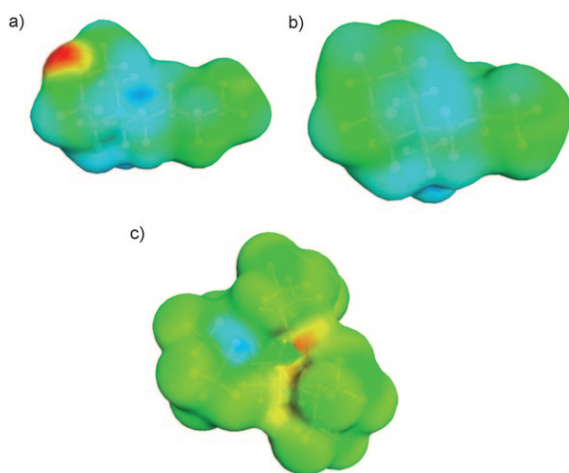


Figure 8. Sigma surfaces of a) $[C_4MMorph]^+$, b) $[C_3MPip]^+$, and c) $[Al(hfip)_4]^-$, visualized by using COSMO-RS^[66,67] and the TURBOMOLE^[62]/(RI)-BP86/TZVP^[64] optimized coordinates. The electron density increases from blue to red according to the following color scale:

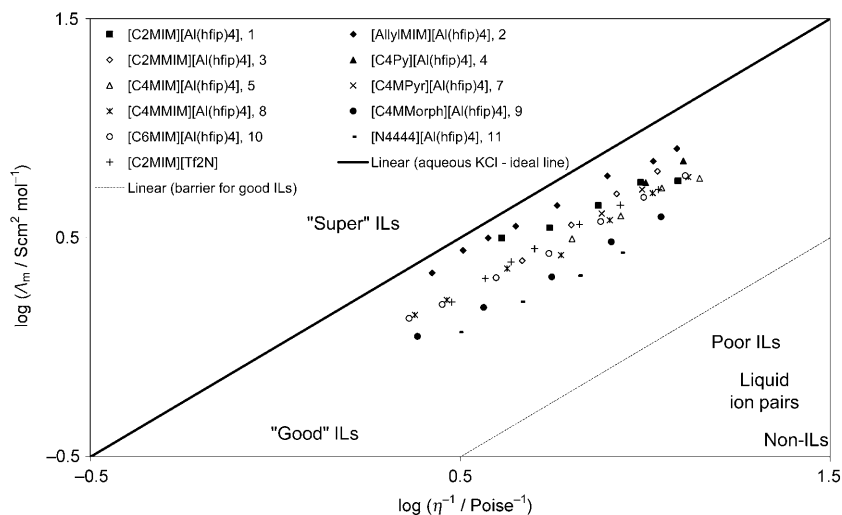


Figure 9. Walden plots for $[Al(hfip)_4]^-$ ILs studied in this work. The thick line is the ideal Walden line, which corresponds to the data for dilute aqueous KCl solution at ambient temperature.^[74] Classification of the ILs in the diagram can be found elsewhere.^[70,71,75] The temperature increases from the lower left corner to the upper right corner. To compare with other ILs, the Walden plot of the classical IL $[C_2MIM][Tf_2N]$ was also made (1-ethyl-3-methylimidazolium bis(trifluoromethylsulfonyl)imide, labeled +).

Static dielectric constants of the $[Al(hfip)_4]^-$ ILs: The static dielectric constant ϵ_S of a liquid provides some insight into the polarity of the liquid as a solvent and, accordingly, has widely been used for this purpose.^[77–79] To complicate the situation for ILs, the ϵ_S of conducting liquids cannot be determined by conventional experiments because the samples are short-circuited by their intrinsic electrical conductance. Dielectric relaxation spectroscopy is the only technique currently available that can provide the ϵ_S of a conducting liquid. The dielectric behavior of an IL is described by the frequency-dependent complex dielectric permittivity $\tilde{\epsilon}(\nu)$. The dielectric constant is defined by the zero-frequency

limit of the real part $\epsilon'(\nu)$ of the complex permittivity, as shown in Equation (6):^[80]

$$\epsilon_S = \lim_{\nu \rightarrow 0} \epsilon'(\nu) \quad (6)$$

We have recently shown that by zero-frequency extrapolation of microwave dielectric data for the dielectric dispersion curve (usually at frequencies >100 MHz) one can extract ϵ_S values for ILs by using an appropriate theoretical or semi-empirical model.^[77,81–83] Similar procedures were applied by Buchner, Hefter and co-workers (their work has been reviewed^[84]).

We used a coaxial reflection technique to determine the complex permittivity of ILs, as described in detail elsewhere.^[77,81] Our instrumentation allows dielectric spectra to be recorded over five decades in frequency from 300 kHz to 20 GHz. However, the relevant segments of the spectra are located above 100 MHz. This is of crucial importance for their parameterization, because at low frequencies parasitic polarizations at the coaxial line/solution interface often perturb the spectra.^[81] The measured dispersion curves involve

a strong primary mode in the 100 MHz to 5 GHz regime, which are parameterized by a Cole–Davidson (CD) relaxation-time distribution.^[80,85]

Weak perturbations of the spectra above 5 GHz indicate a weak second mode parameterized by a conventional Debye function (D).^[80] The experimental dispersion curve was therefore fitted to a bimodal representation with the dominating mode represented by a CD function. This parameterization was then used to extract the static dielectric constant by zero-frequency extrapolation. Unfortunately, the accuracy of dielectric constants obtained in this way is lower than those measured for molecular liquids by an order of magnitude (or more). We estimate an uncertainty of ± 1 for the present data.

The same procedure; that is, a CD ansatz for representing the dominating dielectric mode, has been applied by Buchner, Hefter, and co-workers, but more recently these authors compared dielectric spectra of some ILs with optical Kerr-effect spectra.^[86] By detailed comparison, they concluded that the major mode, originally fitted to a CD ansatz, may be better represented by the so-called Cole–Cole (CC) function.^[87] Note that fits based on a CD and CC representation of the dominating mode possess about the same quality, so that an experimental discrimination is not possible. However, the models differ in their predicted curvature of the low-

frequency wing of the spectrum, which leads to markedly different zero-frequency extrapolations. Typically, the CC model provides dielectric constants that are higher than those extrapolated by the aid of the CD model by 10%. At the present stage, experimental discrimination does not seem possible, and we present the results of both representations in Table 9. The CC result may be considered as an upper limit for the static dielectric constant.

Table 9. Experimentally determined static dielectric constants (ϵ_s) of the $[\text{Al}(\text{hfp})_4]^-$ ILs investigated in this study (column 2–3) as extrapolated by the CC and CD models; all measurements were carried out at 70 °C. Column 4–6: electrical dipole moments (μ) in Debye units ($1 \text{ D} = 3.3 \times 10^{-30} \text{ C m}$) with referred to the center of mass - from single point DFT calculations on (RI)-BP86/SV(P) level by using crystal structure coordinates of the anion (A^-), the cation (C^+) and ion pair (C^+A^-) from asymmetric unit.

IL	ϵ_s CD model	ϵ_s CC model	μ (A^-)	μ (C^+)	μ (C^+A^-)
1	11.7	12.6	2.38	1.66	18.35
2	14.6	17.0	2.99	3.25	31.3
3	16.1	18.0	0.54	1.47	25.4
4	15.3	16.5	2.95	3.32	19.23
5	13.5	14.5	2.68 ^a	4.58 ^a	29.82 ^a
7	16.4	16.6	–	–	–
8	16.8	19.0	–	–	–
9	15.5	16.5	3.72	2.19	38.98
10	16.1	17.3	–	–	–
11	11.5	12.7	3.34 ^b	1.01 ^b	39.76 ^b

[a] Coordinates used for the calculations were taken from the reported crystal structure.^[35] [b] Coordinates used for the calculations were taken from the crystal structure of this IL, which was determined in our group, despite the high final R1 value (0.1129) (not published yet).

Traditional dielectric theory is used to convert the macroscopic dielectric constant into molecular dipole moments by using Onsager theory and its descendants.^[80] Although the same has been done for ILs,^[86] Onsager's procedure has been questioned.^[77,88] The dipole moment of a charged particle depends on the reference frame used, and there is mounting evidence that the usual procedure that relates the dipole moment to the center of mass seems to yield little meaningful results. In addition, in contrast to molecular liquids, the dielectric constant of a charged system is known to be affected by translational motions,^[89] but deconvolution into rotational and translational contributions is not possible experimentally. Finally, in the present case both the cation and anion may contribute to the dielectric constant. In particular, the molecular conformation of the anion in the crystal sufficiently deviates from tetrahedral symmetry to give dipole moments of the order of 2–3.5 D (Table 9). In light of these arguments, it is not possible to draw definite conclusions regarding molecular dipole moments of the ions.

Nevertheless, examination of the results in Table 9 reveals highly interesting features. Based on the apparent low polarity of the anion, one may expect that the dielectric constants of $[\text{Al}(\text{hfp})_4]^-$ correspond to those reported by us earlier for $[\text{Tf}_2\text{N}]^-$ -based ILs, which are of the order of 10–12 (in the CD representation).^[77] The values for $[\text{Al}(\text{hfp})_4]^-$ -based ILs with the same cations are distinctly higher. One ration-

ale is that the dielectric constant increases with rising temperature, which would be highly unusual.^[86] Another possible scenario is that the $[\text{Al}(\text{hfp})_4]^-$ anions yield a notable contribution due to strong deviations from tetrahedral symmetry. This rationale is supported by the dipole moment of the anion calculated from the crystal structure. A third possibility is the presence of long-lived ion pairs (on the time-scale of molecular reorientation) which have very high dipole moments (Table 9), so that a low concentration may be sufficient to generate a high dielectric constant. However, none of the previous studies have provided evidence for the presence of such pairs.^[84] Discrimination among these options, if possible at all, requires a detailed analysis of the frequency dependence, which is currently underway in our laboratories.

Solubility of hydrogen in the $[\text{Al}(\text{hfp})_4]^-$ ILs: Hydrogen solubilities in three $[\text{Al}(\text{hfp})_4]^-$ RTILs were determined by using medium-pressure NMR spectroscopy.^[90] All measured and calculated ^1H NMR spectra of the dissolved dihydrogen and the $[\text{Al}(\text{hfp})_4]^-$ proton peaks are given in the Supporting Information. The relative concentrations are given in Table 10.

Table 10. Solubility of H_2 in $[\text{Al}(\text{hfp})_4]^-$ ILs and in other solvents previously reported, at 0.101 MPa (1 atm).

Solvent	Density [g mL^{-1}]	$10^3 [\text{H}_2]$ [mol L^{-1}]	Reference
2	1.591 ^[a]	5.23 ^[b]	this work
8	1.532 ^[a]	6.50 ^[b]	this work
10	1.502 ^[a]	5.53 ^[b]	this work
$[\text{C}_4\text{MMIM}][\text{Tf}_2\text{N}]$	1.421 ^[90]	0.86 ^[c]	[90]
$[\text{C}_6\text{MIM}][\text{BF}_4]$	1.14 ^[90]	0.79 ^[c]	[90]
water	0.998 ^[91]	0.81 ^[d]	[92]
methanol	0.791 ^[91]	3.75 ^[d]	[93]
ethanol	0.789 ^[91]	2.98 ^[d]	[93]
toluene	1.496 ^[91]	3.50 ^[d]	[93]

[a] Densities were calculated at 298 K by using the previously described method.^[23] [b] Solubility of H_2 at 0.101 MPa (1 atm) and 298 K, calculated from the solubility at 10.1 MPa, with the assumption that it changes linearly with the partial pressure (the mole fractions at 10.1 MPa are $X = 0.212$, $X = 0.265$, and $X = 0.241$ for **2**, **8**, **10**, respectively). [c] Solubility of H_2 at 0.101 MPa (1 atm) and 298 K. [d] Solubility of H_2 at 0.101 MPa (1 atm) and 293 K.

As seen in Table 10, the hydrogen solubilities for all three $[\text{Al}(\text{hfp})_4]^-$ RTILs at RT and at a pressure of 1 atm lie between 5.23×10^{-3} and $6.5 \times 10^{-3} \text{ mol L}^{-1}$. Hydrogen solubilities in $[\text{Al}(\text{hfp})_4]^-$ ILs are up to 7–8 times higher than ILs bearing similar cations and different anions; for example, $[\text{BF}_4]^-$, $[\text{PF}_6]^-$, $[\text{Tf}_2\text{N}]^-$, $[\text{SbF}_6]^-$, $[\text{CF}_3\text{COO}]^-$, or $[\text{CF}_3\text{SO}_3]^-$.^[90] The difference in hydrogen solubilities is a clear effect of the $[\text{Al}(\text{hfp})_4]^-$ anion with its large fluorinated surface. Moreover, the large anion size leads to larger interstices that probably reach the size necessary to accommodate an H_2 molecule. Table 2, above, shows that most of the ILs crystallize in a distorted NaCl structure that may be described as a cubic close-packed lattice of the anions, with the cations occupying all the octahedral interstices. In such a situation, all

tetrahedral interstices are empty, and likely to be available for incorporation of dihydrogen molecules, if one uses the crystalline structure as a rough, 0th order approximation of the liquid state. It is also noteworthy that the solubility of H_2 in the $[Al(hfip)_4]^-$ RTILs is about twice as high as it is in molecular solvents.

Conclusion

It is possible to prepare low-melting and even room-temperature ILs with the fluorinated alkoxyaluminate anion presented here. The synthesis is optimized and simple, and the products can be obtained in high yield. The required starting substances for the synthesis (Li-aluminate and cation halides) are either commercially available^[94] or easily prepared. The ILs of this anion contain both nonfunctionalized and functionalized cations. The IL with the morpholinium functionalized cation, **9**, exhibits increased viscosities and decreased conductivities, possibly due to stronger, bidirectional cation–anion interactions, as observed in the crystal structure, which shows that it contains an additional short contact between the anion and the functionalized group of the cation. Since stronger anion–cation interactions reduce the mobility of the ions in the liquid phase, these additional contacts may be the reason for the higher viscosities and lower conductivities of IL **9**.

The temperature-dependent viscosities and conductivities of the nonfunctionalized $[Al(hfip)_4]^-$ ILs were investigated on the basis of VFT and Arrhenius theory. A further examination in the context of molecular volume, V_m , allowed physical property– V_m correlations to be provided at various temperatures.

The investigation of IL ionicity by determination of the temperature-dependent Walden product showed that these ILs may be classified as at least “good ILs” and that, for example, $[C_2MIM][Al(hfip)_4]$ is a better IL than $[C_2MIM][NTf_2]$.

$[Al(hfip)_4]$ ILs show very good hydrogen solubilities at 25 °C and 1 atm. $[Al(hfip)_4]$ ILs they may show up to 7–8 times higher hydrogen solubilities than those observed for ILs with widely used anions such as $[BF_4]^-$, $[PF_6]^-$, $[Tf_2N]^-$, $[SbF_6]^-$, $[CF_3COO]^-$, or $[CF_3SO_3]^-$ (see Table 10). Hydrogen solubilities in $[Al(hfip)_4]$ ILs are much higher than those in conventional organic solvents such as methanol, ethanol, or toluene, which suggests that the solubilities of other gases in these ILs may also be high.

The $[Al(hfip)_4]^-$ ILs were found to have widely interesting properties: low melting points and RT liquid state; high conductivities and low viscosities comparable to those of the known Tf_2N^- ILs, and better than BF_4^- and PF_6^- ILs; high ionic constitution; and low basicity and hence weak coordinating ability or high electrochemical stability of the anion (>5.0 V versus Li/Li^+ ; used as electrolyte).^[37] These properties, in conjunction with the thorough understanding of their IL properties based on the V_m correlations, suggest great potential for these ILs in many applications. These ILs could

have interesting uses in reaction media which require hydrogen gas as a substrate. They are also of interest for electrochemistry due to the high electrochemical stability of the anion as well as for the stabilization of redox-active cations. The only problem associated with ILs based on this anion is their incompatibility with water. However, most of the applications cited above necessitate the use of anhydrous conditions, so hydrolysis should not be a real hindrance for these applications. On the other hand, the compounds studied here are not readily biodegradable, which is a drawback for such compounds in open systems. However, modification of the Al ligands, as well as of the cation, may improve the biodegradability and greenness of such compounds in future.

Experimental Section

General: Due to the air and moisture sensitivity of most materials, all manipulations were undertaken with standard vacuum and Schlenk techniques (under vacuum of 0.1 Pa) as well as a glove box with an argon atmosphere (H_2O and $O_2 < 1$ ppm). All solvents were dried by using conventional drying agents, and were distilled afterwards. Solution NMR spectra were recorded at room temperature on a BRUKER AC250 or a BRUKER AVANCE 400 spectrometer; data are given in ppm relative to tetramethylsilane (1H , ^{13}C), $AlCl_3$ (^{27}Al), or $CFCl_3$ (^{19}F), with the solvent signals as a secondary reference. IR spectra were obtained on a ZnS or Diamond ATR unit on a Nicolet Magna IR Spectrometer with 1 cm^{-1} resolution. Raman spectra were recorded in flame-sealed capillaries on a BRUKER RAM II Raman module of the BRUKER VERTEX 70 IR spectrometer with a highly sensitive Ge detector. DSC spectra were measured with a SETARAM DSC 131; to infer the melting temperatures, the onset points have been taken into account.

Measurements for the hydrogen solubilities were performed on a Bruker DRX 400 MHz NMR spectrometer. Hydrogen gas ($>99.99\%$) was supplied by Carbagas and used as received. All measurements were carried out in a sapphire NMR tube^[95] at a pressure of 100 atm after shaking for 8 h (multiple measurements were performed to ensure that the $[H_2]$ had reached its maximum value). Spectra were fitted by using NMRICMA 2.8 (nonlinear least-squares iterative fitting application for MatLab). The integral of the dihydrogen peak ($\approx 4/3$ because of the spin distribution) of the ionic liquid was determined in relation to the peak corresponding to four $[Al(hfip)_4]^-$ protons ($hfip: OCH(CF_3)_2$).

The viscosity was measured with a programmable Brookfield rotation viscosimeter (RVDV-III UCP) under an atmosphere of dry air in a purpose-built glove box (relative humidity below 0.1%, see photo in the Supporting Information.). The temperature of the samples was measured with an external cryostat, so that the measurement of the viscosity was temperature dependent between 0 and 80 °C (if the samples permitted). Accuracy was about ± 0.1 °C.

General procedure for the synthesis of $[Al(hfip)_4]^-$ salts: Equimolar amounts of $Li[Al(hfip)_4]$ and $[Cat]X$ were weighed into a Schlenk vessel. Dry CH_2Cl_2 was added (10 mL solvent for each gram of $Li[Al(hfip)_4]$ used). The mixture was stirred at room temperature for 24 h, and then filtered over siliceous earth through a Schlenk frit (siliceous earth in the Schlenk frit was washed several times with CH_2Cl_2 and dried in vacuum by heating to 350 to 500 °C for 3–4 h before filtration). The solvent was removed by vacuum distillation. The product was rinsed with dry hexane and dried in a high vacuum (0.1 Pa) for 1 day.

Experimental data for **1:** $Li[Al(hfip)_4]$ (6.94 g, 9.88 mmol), $[C_2MIM]Br$ (1.89 g, 9.88 mmol); isolated yield: 7.97 g (88%). 1H NMR (200.13 MHz, CD_2Cl_2): $\delta = 1.53$ (t, 3H, CH_3), 3.88 (s, 3H, $N(CH_3)$), 4.18 (q, 2H, $N(CH_2)$), 4.53 (sep, $^3J(H,F) = 5.9$ Hz, 4H, CH), 7.25 (m, 2H, CH), 8.65 ppm (s, $\omega^{1/2} = 4.5$ Hz, 1H, CH); ^{19}F NMR (188.31 MHz, CD_2Cl_2): $\delta =$

-77.4 ppm (d, ³J(F,H)=5.8 Hz, CF₃); ²⁷Al NMR (104.27 MHz, [D₆]acetone): δ=60.5 ppm (s, ω^{1/2}=78 Hz); Raman: ν̄=435, 443, 488, 503, 524, 536, 551, 569, 597, 623, 644, 653, 672, 697, 724, 762, 804, 858, 891, 960, 979, 1024, 1054, 1090, 1108, 1142, 1153, 1187, 1225, 1251, 1269, 1296, 1335, 1381, 1422, 1433, 1457, 1476, 1487, 1504, 1572, 2716, 2755, 2842, 2903, 2934, 2958, 2976, 3006, 3082, 3140, 3187 cm⁻¹. IR (diamond ATR, Attenuated Total Reflection): ν̄=427 (m), 439 (m), 522 (m), 535 (w), 568 (m), 624 (w), 651 (w), 684 (s), 724 (w), 743 (m), 760 (w), 792 (m), 854 (m), 890 (m), 959 (vw), 1027 (w), 1095 (s), 1168 (vs), 1207 (m), 1262 (m), 1292 (m), 1377 (m), 1432 (vw), 1569 (w), 1598 (w), 2324 (vw), 2360 (vw), 2905 (vw), 3083 (vw), 3166 (vw) cm⁻¹; m.p. (DSC): 31 °C.

Experimental data for 2: Li[Al(hfip)₄] (4 g, 5.69 mmol), [AllylMIM]Cl (0.904 g, 5.69 mmol); isolated yield: 4.336 g (93%). ¹H NMR (200.13 MHz, CD₂Cl₂): δ=3.89 (s, 3H, N(CH₃)), 4.54 (sep, ³J(H,F)=6 Hz, 4H, CH), 4.71 (d, ³J(H,H)=6.4 Hz, 2H, CH₂), 5.49 (m, 2H, N(CH₂)), 5.95 (m, 1H, CH), 7.25 (m, 2H, CH), 8.59 ppm (m, ω^{1/2}=4 Hz, 1H, CH); ¹⁹F NMR (188.31 MHz, CD₂Cl₂): δ=-77.4 ppm (d, ³J(F,H)=6.2 Hz, CF₃); ²⁷Al NMR (104.27 MHz, CD₂Cl₂): δ=60.2 ppm (s, ω^{1/2}=78 Hz); Raman: ν̄=500, 524, 568, 624, 695, 725, 761, 857, 889, 919, 954, 1025, 1104, 1187, 1297, 1380, 1416, 1457, 1570, 1652, 2716, 2903, 2974, 3004, 3037, 3106, 3185 cm⁻¹; IR (diamond ATR): ν̄=426 (m), 438 (m), 522 (m), 535 (w), 567 (m), 626 (w), 685 (s), 725 (vw), 743 (w), 760 (vw), 789 (m), 852 (s), 889 (m), 952 (w), 990 (w), 1029 (vw), 1094 (vs), 1174 (vs), 1210 (s), 1260 (m), 1291 (m), 1375 (m), 1428 (w), 1454 (vw), 1566 (w), 1575 (w), 1598 (vw), 2902 (vw), 3085 (vw), 3163 (vw) cm⁻¹; m.p. (DSC): 12 °C.

Experimental data for 3: Li[Al(hfip)₄] (10 g, 14.24 mmol), [C₂MMIM]Br (2.92 g, 14.24 mmol); isolated yield: 11.34 g (97%). ¹H NMR (200.13 MHz, CD₂Cl₂): δ=1.48 (t, 3H, CH₃), 2.58 (s, 3H, CH₃), 3.77 (s, 3H, N(CH₃)), 4.09 (q, 2H, N(CH₂)), 4.51 (sep, ³J(H,F)=6.1 Hz, 4H, CH), 7.2 ppm (m, 2H, CH); ¹⁹F NMR (188.31 MHz, CD₂Cl₂): δ=-77.3 ppm (d, ³J(F,H)=6.2 Hz, CF₃); ²⁷Al NMR (104.27 MHz, [D₆]acetone): δ=60.5 ppm (s, ω^{1/2}=97 Hz); Raman: ν̄=437, 526, 538, 571, 599, 699, 764, 802, 859, 894, 962, 1026, 1092, 1191, 1255, 1298, 1337, 1384, 1424, 1459, 1574, 2719, 2760, 2846, 2902, 2937, 2960, 2978, 3189 cm⁻¹; IR (diamond ATR): ν̄=433 (m), 442 (m), 521 (m), 534 (w), 568 (m), 667 (m), 684 (s), 712 (vw), 726 (w), 740 (m), 785 (m), 803 (m), 853 (s), 889 (m), 955 (vw), 1094 (s), 1170 (vs), 1206 (m), 1262 (m), 1289 (m), 1381 (m), 1537 (w), 1590 (w), 1982 (vw), 2896 (vw), 3168 (vw) cm⁻¹; m.p. (DSC): 39 °C.

Experimental data for 4: Li[Al(hfip)₄] (10 g, 14.24 mmol), [C₂Py]Cl (2.445 g, 14.24 mmol); isolated yield: 11.36 g (96%). ¹H NMR (200.13 MHz, CD₂Cl₂): δ=0.99 (t, 3H, CH₃), 1.41 (sex, 2H, CH₂), 2.01 (quin, 2H, CH₂), 4.52 (sep, ³J(H,F)=6.1 Hz, 4H, CH), 4.72 (t, 2H, N(CH₂)), 8.08 (t, 2H, CH), 8.5 (t, 1H, CH), 9.02 ppm (m, ω^{1/2}=12 Hz, 2H, N(CH)); ¹⁹F NMR (188.31 MHz, CD₂Cl₂): δ=-77.3 ppm (d, ³J(F,H)=6.2 Hz, CF₃); ²⁷Al NMR (104.27 MHz, CD₂Cl₂): δ=60.4 ppm (s, ω^{1/2}=92 Hz); Raman: ν̄=431, 469, 503, 523, 536, 570, 614, 649, 693, 740, 762, 783, 813, 829, 856, 889, 910, 946, 987, 1031, 1051, 1099, 1119, 1146, 1175, 1218, 1262, 1293, 1378, 1449, 1487, 1505, 1587, 1638, 1652, 2638, 2719, 2757, 2887, 2915, 2947, 2979, 3055, 3109, 3172 cm⁻¹; IR (diamond ATR): ν̄=428 (m), 443 (m), 501 (w), 521 (m), 535 (w), 568 (m), 683 (s), 725 (w), 735 (w), 766 (m), 792 (m), 854 (s), 890 (m), 958 (vw), 1030 (w), 1095 (s), 1166 (vs), 1205 (m), 1239 (m), 1264 (m), 1291 (m), 1380 (m), 1442 (vw), 1462 (vw), 1490 (w), 1503 (vw), 1587 (vw), 1637 (w), 2897 (vw), 2943 (vw), 2979 (vw), 3075 (vw), 3093 (vw), 3143 (vw) cm⁻¹; m.p. (DSC): 36 °C.

Experimental data for 5: Li[Al(hfip)₄] (10 g, 14.24 mmol), [C₄MIM]Cl (2.49 g, 14.24 mmol); isolated yield: 10.81 g (91%). ¹H NMR (400.17 MHz, CD₂Cl₂): δ=0.97 (t, 3H, CH₃), 1.37 (sex, 2H, CH₂), 1.84 (quin, 2H, CH₂), 3.89 (s, 3H, N(CH₃)), 4.10 (t, 2H, N(CH₂)), 4.54 (sep, ³J(H,F)=5.9 Hz, 4H, CH), 7.25 (m, 2H, CH), 8.52 ppm (m, ω^{1/2}=4.2 Hz, 1H, CH); ¹⁹F NMR (376.53 MHz, CD₂Cl₂): δ=-77.4 ppm (d, ³J(F,H)=6.2 Hz, CF₃); ²⁷Al NMR (104.27 MHz, CD₂Cl₂): δ=60.2 ppm (s, ω^{1/2}=83 Hz); Raman: ν̄=413, 497, 524, 536, 569, 601, 624, 653, 696, 762, 825, 858, 886, 909, 949, 1023, 1055, 1107, 1194, 1261, 1293, 1338, 1381, 1420, 1432, 1449, 1463, 1503, 1572, 2717, 2745, 2840, 2887, 2905, 2948, 2974, 3084, 3188 cm⁻¹; IR (diamond ATR): ν̄=428 (m), 439 (m), 521 (m), 535

(w), 569 (m), 625 (w), 651 (w), 683 (s), 725 (vw), 744 (m), 754 (vw), 793 (m), 854 (s), 890 (m), 948 (vw), 1027 (w), 1094 (s), 1166 (vs), 1204 (m), 1235 (m), 1263 (m), 1292 (m), 1379 (m), 1431 (vw), 1464 (vw), 1568 (w), 1599 (w), 2899 (vw), 2975 (vw), 3083 (vw), 3167 (vw) cm⁻¹; m.p. (DSC): 40 °C.

Experimental data for 6: Li[Al(hfip)₄] (6 g, 8.55 mmol), [C₃MPip]Br (1.90 g, 8.55 mmol); isolated yield: 6.80 g (95%). ¹H NMR (200.13 MHz, CD₂Cl₂): δ=1.05 (t, 3H, CH₃), 1.73 (m, 4H, CH₂), 1.90 (m, 4H, CH₂), 2.98 (s, 3H, N(CH₃)), 3.16 (m, 2H, N(CH₂)), 3.25 (t, 4H, N(CH₂)), 4.52 ppm (sep, ³J(H,F)=6.1 Hz, 4H, CH); ¹⁹F NMR (188.31 MHz, CD₂Cl₂): δ=-77.3 ppm (d, ³J(F,H)=6.3 Hz, CF₃); ²⁷Al NMR (104.27 MHz, [D₆]acetone): δ=60.5 ppm (s, ω^{1/2}=63 Hz); Raman: ν̄=439, 477, 492, 524, 536, 550, 569, 599, 695, 715, 761, 790, 841, 858, 878, 913, 940, 981, 991, 1036, 1086, 1099, 1115, 1150, 1189, 1221, 1234, 1280, 1297, 1312, 1379, 1413, 1446, 1457, 1487, 2664, 2717, 2758, 2793, 2895, 2938, 2957, 2986, 3043 cm⁻¹; IR (diamond ATR): ν̄=522 (m), 534 (m), 541 (m), 603 (w), 623 (m), 631 (m), 652 (m), 656 (m), 684 (s), 743 (m), 755 (w), 823 (m), 829 (m), 863 (m), 890 (m), 959 (m), 990 (m), 1020 (s), 1056 (m), 1091 (vs), 1133 (s), 1148 (vs), 1164 (s), 1180 (s), 1204 (m), 1214 (m), 1264 (m), 1288 (m), 1336 (vw), 1382 (m), 1431 (vw), 1464 (vw), 1471 (vw), 1571 (w), 1603 (w), 2887 (vw), 2949 (vw), 2977 (vw), 3180 (vw) cm⁻¹; m.p. (DSC): 69 °C.

Experimental data for 7: Li[Al(hfip)₄] (10 g, 14.24 mmol), [C₄MPyr]Cl (2.53 g, 14.24 mmol); isolated yield: 11.09 g (93%). ¹H NMR (400.17 MHz, CD₂Cl₂): δ=1.0 (t, 3H, CH₃), 1.42 (sex, 2H, CH₂), 1.73 (quin, 2H, CH₂), 2.26 (m, 4H, CH₂), 3.0 (s, 3H, N(CH₃)), 3.2 (m, 2H, N(CH₂)), 3.42 (m, 4H, N(CH₂)), 4.53 ppm (sep, ³J(H,F)=6.1 Hz, 4H, CH); ¹⁹F NMR (376.53 MHz, CD₂Cl₂): δ=-77.3 ppm (d, ³J(F,H)=6 Hz, CF₃); ²⁷Al NMR (104.27 MHz, CD₂Cl₂): δ=60.4 ppm (s, ω^{1/2}=112 Hz); Raman: ν̄=412, 427, 441, 473, 493, 524, 536, 551, 569, 628, 695, 728, 761, 799, 822, 858, 905, 928, 965, 1008, 1020, 1032, 1052, 1061, 1098, 1122, 1184, 1231, 1239, 1262, 1296, 1317, 1379, 1460, 1501, 2717, 2758, 2792, 2891, 2908, 2957, 2982, 3114 cm⁻¹; IR (diamond ATR): ν̄=426 (m), 440 (m), 522 (m), 534 (w), 567 (m), 684 (s), 725 (w), 743 (vw), 760 (w), 790 (m), 853 (s), 889 (m), 929 (w), 966 (vw), 1006 (w), 1031 (w), 1094 (s), 1171 (vs), 1206 (m), 1263 (m), 1291 (m), 1377 (m), 1431 (vw), 1468 (vw), 1482 (vw), 1530 (vw), 1549 (vw), 1585 (vw), 2342 (w), 2359 (w), 2892 (vw), 2948 (vw) cm⁻¹; m.p. (DSC): 50 °C.

Experimental data for 8: Li[Al(hfip)₄] (4 g, 5.69 mmol), [C₄MMIM]Br (1.328 g, 5.69 mmol); isolated yield: 4.612 g (95.4%). ¹H NMR (400.17 MHz, CDCl₃/25% Et₂O): δ=0.76 (t, 3H, CH₃), 1.16 (sex, 2H, CH₂), 1.56 (quin, 2H, CH₂), 2.37 (s, 3H, CH₃), 3.56 (s, 3H, N(CH₃)), 3.82 (t, 2H, N(CH₂)), 4.27 (sep, ³J(H,F)=6.1 Hz, 4H, CH), 7.01(d, 1H, CH), 7.08 ppm (d, 1H, CH); ¹⁹F NMR (376.53 MHz, CDCl₃/25% Et₂O): δ=-77.7 ppm (d, ³J(F,H)=6.1 Hz, CF₃); ²⁷Al NMR (104.27 MHz, CDCl₃/25% Et₂O): δ=60.2 ppm (s, ω^{1/2}=148 Hz); Raman: ν̄=431, 526, 538, 570, 610, 630, 698, 727, 763, 827, 858, 888, 911, 964, 1051, 1102, 1187, 1270, 1297, 1343, 1381, 1453, 1517, 2716, 2754, 2889, 2917, 2949, 2977, 3164, 3195 cm⁻¹; IR (diamond ATR): ν̄=440 (w), 522 (w), 535 (vw), 568 (w), 670 (vw), 686 (m), 726 (vw), 742 (w), 759 (vw), 794 (m), 856 (m), 890 (m), 1100 (s), 1184 (vs), 1212 (s), 1224 (s), 1262 (m), 1292 (m), 1377 (m), 1425 (vw), 1465 (vw), 1540 (w), 1591 (w), 2341 (w), 2361 (w), 2886 (w), 2945 (vw), 2973 (w), 3164 (vw), 3193 (vw) cm⁻¹; m.p. (DSC): 0 °C.

Experimental data for 9: Li[Al(hfip)₄] (5.43 g, 7.73 mmol), [C₄MMorph]Br (1.84 g, 7.73 mmol); isolated yield: 5.87 g (89%). ¹H NMR (400.17 MHz, CD₂Cl₂): δ=1.02 (t, 3H, CH₃), 1.44 (sex, 2H, CH₂), 1.72 (quin, 2H, CH₂), 3.11 (s, 3H, N(CH₃)), 3.34 (m, 6H, N(CH₂)), 3.98 (m, 4H, O(CH₂)), 4.53 ppm (sep, ³J(H,F)=6 Hz, 4H, CH); ¹⁹F NMR (376.53 MHz, CD₂Cl₂): δ=-77.3 ppm (d, ³J(F,H)=6.2 Hz, CF₃); ²⁷Al NMR (104.27 MHz, CD₂Cl₂): δ=60.2 ppm (s, ω^{1/2}=115 Hz); Raman: ν̄=447, 501, 523, 535, 567, 622, 695, 717, 761, 819, 857, 891, 914, 945, 981, 1016, 1056, 1098, 1140, 1179, 1236, 1307, 1320, 1379, 1453, 1480, 2548, 2716, 2888, 2908, 2952, 2988 cm⁻¹; IR (diamond ATR): ν̄=426 (m), 443 (m), 521 (m), 534 (w), 567 (m), 622 (vw), 635 (w), 683 (s), 723 (vw), 742 (vw), 760 (w), 790 (m), 852 (s), 888 (m), 913 (w), 944 (vw), 981 (w), 1021 (w), 1040 (w), 1062 (m), 1092 (s), 1121 (m), 1170 (vs), 1208 (m), 1261 (m), 1290 (m), 1375 (m), 1431 (vw), 1462 (w), 1479 (w), 2359 (vw), 2888 (vw), 2981 (vw) cm⁻¹; m.p. (DSC): 31 °C.

Table 11. Crystallographic details for **1**, **2**, **3**, **4**, **6**, and **9** at given temperatures refined by full-matrix least-squares on F^2 .^[96]

	1	2	3	4	6	9
chemical formula	C ₁₈ H ₁₅ AlF ₂₄ N ₂ O ₄	C ₁₉ H ₁₅ AlF ₂₄ N ₂ O ₄	C ₁₉ H ₁₇ AlF ₂₄ N ₂ O ₄	C ₂₁ H ₁₈ AlF ₂₄ NO ₄	C ₂₁ H ₂₄ AlF ₂₄ NO ₄	C ₂₁ H ₂₄ AlF ₂₄ NO ₅
formula weight [g mol ⁻¹]	806.3	818.31	820.33	831.34	837.39	853.39
T [K]	113(2)	100(2)	120(2)	113(2)	113(2)	113(2)
λ [Å]	0.71073	0.71073	0.71073	0.71073	0.71073	0.71073
crystal system	triclinic	monoclinic	monoclinic	monoclinic	orthorhombic	orthorhombic
space group	<i>P</i> $\bar{1}$	<i>P</i> 2 ₁ / <i>c</i>	<i>P</i> 2 ₁ / <i>n</i>	<i>P</i> 2 ₁ / <i>c</i>	<i>P</i> 2 ₁ 2 ₁ 2 ₁	<i>P</i> <i>na</i> 2 ₁
<i>a</i> [Å]	10.988(2)	17.6794(6)	8.8078(18)	30.194(6)	9.0454(6)	19.968(4)
<i>b</i> [Å]	15.529(3)	11.0667(5)	28.307(6)	11.519(2)	18.2184(11)	9.5591(19)
<i>c</i> [Å]	17.481(4)	17.0411(6)	12.682(3)	17.597(4)	19.5343(15)	17.151(3)
α [°]	89.06(3)	90	90	90	90	90
β [°]	89.97(3)	113.7305(9)	106.24(3)	95.82(3)	90	90
γ [°]	90.00(3)	90	90	90	90	90
<i>V</i> [Å ³]	2982.3(10)	3052.3(2)	3035.8(11)	6089(2)	3219.1(4)	3273.8(11)
<i>Z</i>	4	4	4	8	4	4
ρ _{calc} [Mg m ⁻³]	1.796	1.781	1.795	1.814	1.728	1.731
μ [mm ⁻¹]	0.248	0.244	0.246	0.245	0.232	0.233
absorption correction	none	multiscan	multiscan	multiscan	multiscan	none
<i>F</i> (000)	1592	1616	1624	3296	1672	1704
crystal size [mm]	0.2 × 0.2 × 0.1	0.4 × 0.8 × 0.3	0.2 × 0.1 × 0.5	0.2 × 0.1 × 0.2	0.2 × 0.2 × 0.1	0.2 × 0.3 × 0.2
θ range for data collection [°]	3.21 to 20.82	3.02 to 27.47	3.23 to 23.26	3.02 to 20.82	3.06 to 21.96	3.13 to 24.41
index ranges	-10 ≤ <i>h</i> ≤ 10 -15 ≤ <i>k</i> ≤ 15 -17 ≤ <i>l</i> ≤ 17	-22 ≤ <i>h</i> ≤ 22 -14 ≤ <i>k</i> ≤ 14 -22 ≤ <i>l</i> ≤ 22	-9 ≤ <i>h</i> ≤ 9 -31 ≤ <i>k</i> ≤ 31 -14 ≤ <i>l</i> ≤ 14	-30 ≤ <i>h</i> ≤ 30 -11 ≤ <i>k</i> ≤ 11 -17 ≤ <i>l</i> ≤ 17	-9 ≤ <i>h</i> ≤ 9 -19 ≤ <i>k</i> ≤ 19 -20 ≤ <i>l</i> ≤ 20	-23 ≤ <i>h</i> ≤ 23 -11 ≤ <i>k</i> ≤ 11 -19 ≤ <i>l</i> ≤ 19
reflections collected	24129	57146	29697	50452	15831	40448
independent reflections	6053 [<i>R</i> _{int} = 0.0454]	6977 [<i>R</i> _{int} = 0.0317]	4347 [<i>R</i> _{int} = 0.0376]	6348 [<i>R</i> _{int} = 0.0877]	3869 [<i>R</i> _{int} = 0.0406]	5376 [<i>R</i> _{int} = 0.0324]
reflections with <i>I</i> > 2σ(<i>I</i>)	4944	5869	3433	4359	3118	4821
data/restraints/parameters	6053/0/884	6977/21/530	4347/21/533	6348/0/919	3869/814/634	5376/1/485
goodness-of-fit on <i>F</i> ²	<i>S</i> = 1.080	<i>S</i> = 1.025	<i>S</i> = 1.073	<i>S</i> = 1.010	<i>S</i> = 1.050	<i>S</i> = 1.076
<i>R</i> indices [<i>I</i> > 2σ(<i>I</i>)]	<i>R</i> ₁ = 0.0726 <i>wR</i> ₂ = 0.1955	<i>R</i> ₁ = 0.0353 <i>wR</i> ₂ = 0.0850	<i>R</i> ₁ = 0.0380 <i>wR</i> ₂ = 0.0853	<i>R</i> ₁ = 0.0383 <i>wR</i> ₂ = 0.0731	<i>R</i> ₁ = 0.0446 <i>wR</i> ₂ = 0.1055	<i>R</i> ₁ = 0.0298 <i>wR</i> ₂ = 0.0710
<i>R</i> indices (all data)	<i>R</i> ₁ = 0.0892 <i>wR</i> ₂ = 0.2270	<i>R</i> ₁ = 0.0431 <i>wR</i> ₂ = 0.0884	<i>R</i> ₁ = 0.0512 <i>wR</i> ₂ = 0.0920	<i>R</i> ₁ = 0.0710 <i>wR</i> ₂ = 0.0837	<i>R</i> ₁ = 0.0615 <i>wR</i> ₂ = 0.1171	<i>R</i> ₁ = 0.0348 <i>wR</i> ₂ = 0.0730
weighting scheme ^[a] <i>w</i> / <i>y</i>	0.14/9	0.0329/1.9851	0.0338/2.1602	0.0325/2.873	0.0648/1.6456	0.0391/0.7
largest diff. peak and hole [e Å ⁻³]	0.312 and -0.417	0.318 and -0.244	0.263 and -0.227	0.238 and -0.229	0.375 and -0.247	0.216 and -0.230

[a] $w = 1/[\sigma^2(F_o^2) + (xP)^2 + yP]$, in which $P = (F_o^2 + 2F_c^2)/3$.

Experimental data for 10: Li[Al(hfip)₄] (4 g, 5.69 mmol), [C₆MIM]Cl (1.155 g, 5.69 mmol); isolated yield: 4.768 g (97.05%). ¹H NMR (200.13 MHz, CD₂Cl₂): δ = 0.89 (t, 3H, CH₃), 1.33 (m, 6H, CH₂), 1.85 (quin, 2H, CH₂), 3.89 (s, 3H, N(CH₃)), 4.1 (t, 2H, N(CH₂)), 4.54 (sep, ³*J*(H,F) = 6.0 Hz, 4H, CH), 7.24 (m, 2H, CH), 8.62 ppm (s, 1H, CH); ¹⁹F NMR (188.31 MHz, CD₂Cl₂): δ = -77.3 ppm (d, ³*J*(F,H) = 6.0 Hz, CF₃); ²⁷Al NMR (104.27 MHz, CD₂Cl₂): δ = 60.3 ppm (s, *w*_{1/2} = 86 Hz); Raman: $\tilde{\nu}$ = 525, 568, 598, 623, 695, 762, 857, 892, 1025, 1108, 1189, 1294, 1339, 1382, 1419, 1448, 1496, 1571, 2719, 2907, 2972, 3185 cm⁻¹; IR (diamond ATR): $\tilde{\nu}$ = 442 (w), 522 (w), 535 (vw), 568 (w), 624 (w), 651 (vw), 686 (m), 726 (vw), 742 (w), 760 (vw), 794 (m), 856 (m), 890 (m), 1027 (vw), 1100 (s), 1185 (vs), 1213 (s), 1225 (s), 1261 (m), 1292 (m), 1377 (m), 1433 (vw), 1464 (vw), 1472 (vw), 1567 (w), 1596 (vw), 2878 (vw), 2938 (w), 2966 (w), 3089 (vw), 3122 (vw), 3162 (vw) cm⁻¹; m.p. (DSC): 5 °C.

Experimental data for [(2-HOEt)MIM][Al(hfip)₄]: The information and spectral data for [(2-HOEt)MIM][Al(hfip)₄] given below are from a clean synthesis batch. Unfortunately, several attempts to repeat the procedure were not successful; in that the product could not be reproduced with the same purity as the first synthesis. The spectra of the products from several batches are given in the Supporting Information.

Li[Al(hfip)₄] (10 g, 14.24 mmol), [(2-HOEt)MIM]Cl (2.316 g, 14.24 mmol); isolated yield: 9.84 g (84%). ¹H NMR (200.13 MHz, CD₂Cl₂): δ = 3.85 (s, 3H, N(CH₃)), 3.99 (t, 2H, CH₂), 4.15 (t, 2H, N(CH₂)), 4.5 (sep, ³*J*(H,F) = 6.2 Hz, 4H, CH), 7.15 (m, 1H, CH), 7.21 (m, 1H, CH), 8.69 ppm (s, *w*_{1/2} = 4 Hz, 1H, CH); ¹⁹F NMR (188.31 MHz, CD₂Cl₂): δ = -77.3 ppm (d, ³*J*(F,H) = 6.2 Hz, CF₃); ²⁷Al NMR (104.27 MHz, [D₆]acetone): δ = 60.5 ppm (s, *w*_{1/2} = 103 Hz); Raman: $\tilde{\nu}$ =

417, 442, 482, 500, 524, 536, 568, 599, 624, 653, 688, 696, 723, 738, 762, 857, 890, 918, 950, 1023, 1039, 1095, 1185, 1271, 1293, 1341, 1382, 1420, 1454, 1474, 1503, 1572, 2716, 2739, 2900, 2973, 3115, 3184 cm⁻¹; IR (diamond ATR): $\tilde{\nu}$ = 427 (m), 437 (m), 522 (m), 535 (m), 566 (m), 622 (m), 653 (m), 685 (s), 722 (w), 740 (m), 785 (m), 852 (s), 889 (m), 950 (vw), 1029 (m), 1093 (s), 1171 (vs), 1209 (m), 1259 (m), 1289 (m), 1375 (m), 1431 (vw), 1452 (vw), 1567 (w), 1593 (w), 2339 (w), 2362 (w), 2894 (vw), 2961 (vw), 3166 (vw) cm⁻¹; m.p. (DSC): 21 °C.

Acknowledgements

This work was supported by the Deutsche Forschungsgemeinschaft DFG (SPP 1191 and Normalverfahren) and the Albert-Ludwigs-Universität Freiburg, Germany.

- [1] P. Wasserscheid, W. Keim, *Angew. Chem.* **2000**, *112*, 3926–3945; *Angew. Chem. Int. Ed.* **2000**, *39*, 3772–3789.
- [2] P. Wasserscheid, T. Welton, *Ionic Liquids in Synthesis*, Wiley-VCH, Weinheim, **2003**.
- [3] H. Shobukawa, H. Tokuda, A. B. H. Susan, M. Watanabe, *Electrochim. Acta* **2005**, *50*, 3872–3877.
- [4] H. Shobukawa, H. Tokuda, S.-i. Tabata, M. Watanabe, *Electrochim. Acta* **2004**, *50*, 305–309.

- [5] S. Seki, Y. Kobayashi, H. Miyashiro, Y. Ohno, A. Usami, Y. Mita, M. Watanabe, N. Terada, *Chem. Commun.* **2006**, 544–545.
- [6] M. C. Buzzeeo, R. G. Evans, R. G. Compton, *ChemPhysChem* **2004**, *5*, 1106–1120.
- [7] A. Lewandowski, M. Galinski, *J. Phys. Chem. Solids* **2004**, *65*, 281–286.
- [8] B. O'Regan, M. Grätzel, *Nature* **1991**, *353*, 737–740.
- [9] P. Wang, S. M. Zakeeruddin, P. Comte, I. Exnar, M. Grätzel, *J. Am. Chem. Soc.* **2003**, *125*, 1166–1167.
- [10] P. Wang, S. M. Zakeeruddin, J.-E. Moser, M. Grätzel, *J. Phys. Chem. B* **2003**, *107*, 13280–13285.
- [11] P. Wang, S. M. Zakeeruddin, M. Shaik, R. Humphry-Baker, M. Grätzel, *Chem. Mater.* **2004**, *16*, 2694–2696.
- [12] C. A. Angell, W. Xu, *Science* **2003**, *302*, 422–425.
- [13] F. Mazille, Z. Fei, D. Kuang, D. Zhao, S. M. Zakeeruddin, M. Grätzel, P. J. Dyson, *Inorg. Chem.* **2006**, *45*, 1585–1590.
- [14] S. Zein El-Abedin, F. Endres, *ChemPhysChem* **2006**, *7*, 58–61.
- [15] A. Bösmann, T. J. S. Schubert in *Novel Pairs of Working Substances for Absorption Heat Pumps, Absorption Refrigeration Machines and Heat Transformers*, PCT Int. Appl., WO 2005113702, **2005**.
- [16] S. Carda-Broch, A. Berthod, D. W. Armstrong, *Anal. Bioanal. Chem.* **2003**, *375*, 191–199.
- [17] H. Itoh, K. Naka, Y. Chujo, *J. Am. Chem. Soc.* **2004**, *126*, 3026–3027.
- [18] B. S. Lee, Y. S. Chi, J. K. Lee, I. S. Choi, C. E. Song, S. K. Namgoong, S.-g. Lee, *J. Am. Chem. Soc.* **2004**, *126*, 480–481.
- [19] M. Antonietti, D. Kuang, B. Smarsly, Y. Zhou, *Angew. Chem.* **2004**, *116*, 5096–5100; *Angew. Chem. Int. Ed.* **2004**, *43*, 4988–4992.
- [20] K. M. Docherty, J. K. Dixon, C. F. Kulpa, *Biodegradation* **2007**, *18*, 481–493.
- [21] J. R. Harjani, J. Farrell, M. T. Garcia, R. D. Singer, P. J. Scammells, *Green Chem.* **2009**, *11*, 821–829.
- [22] I. Krossing, J. M. Slattery, C. Daguene, P. J. Dyson, A. Oleinikova, H. Weingärtner, *J. Am. Chem. Soc.* **2006**, *128*, 13427–13434.
- [23] U. Preiss, J. M. Slattery, I. Krossing, *Ind. Eng. Chem. Res.* **2009**, *48*, 2290–2296.
- [24] J. M. Slattery, C. Daguene, P. J. Dyson, T. J. S. Schubert, I. Krossing, *Angew. Chem.* **2007**, *119*, 5480–5484; *Angew. Chem. Int. Ed.* **2007**, *46*, 5384–5388.
- [25] I. Krossing, I. Raabe, *Angew. Chem.* **2004**, *116*, 2116–2142; *Angew. Chem. Int. Ed.* **2004**, *43*, 2066–2090.
- [26] T. S. Cameron, A. Decken, I. Dionne, M. Fang, I. Krossing, J. Passmore, *Chem. Eur. J.* **2002**, *8*, 3386–3401.
- [27] A. Reisinger, I. Krossing, *Angew. Chem.* **2003**, *115*, 5903–5906; *Angew. Chem. Int. Ed.* **2003**, *42*, 5725–5728.
- [28] A. Reisinger, N. Trapp, I. Krossing, S. Altmannshofer, V. Herz, M. Presnitz, W. Scherer, *Angew. Chem.* **2007**, *119*, 8445–8449; *Angew. Chem. Int. Ed.* **2007**, *46*, 8295–8298.
- [29] M. Gonsior, I. Krossing, *Chem. Eur. J.* **2006**, *12*, 1997–2008.
- [30] A. Adolf, M. Gonsior, I. Krossing, *J. Am. Chem. Soc.* **2002**, *124*, 7111–7116.
- [31] S. Antonijevic, I. Raabe, I. Krossing, *Chem. Eur. J.* **2007**, *13*, 7510–7522.
- [32] G. Santiso-Quiñones, A. Reisinger, J. Slattery, I. Krossing, *Chem. Commun.* **2007**, 5046–5048.
- [33] T. J. Barbarich, S. T. Handy, S. M. Miller, O. P. Anderson, P. A. Grieco, S. H. Strauss, *Organometallics* **1996**, *15*, 3776–3778.
- [34] S. M. Ivanova, B. G. Nolan, Y. Kobayashi, S. M. Miller, O. P. Anderson, S. H. Strauss, *Chem. Eur. J.* **2001**, *7*, 503–510.
- [35] T. Timofte, S. Pitula, A. V. Mudring, *Inorg. Chem.* **2007**, *46*, 10938–10940.
- [36] A. Babai, A. V. Mudring, *Z. Anorg. Allg. Chem.* **2006**, *632*, 1956–1958.
- [37] S. Tsujioka, B. G. Nolan, H. Takase, B. P. Fauber, S. H. Strauss, *J. Electrochem. Soc.* **2004**, *151*, A1418–A1423.
- [38] I. Raabe, K. Wagner, K. Guttische, M. Wang, M. Grätzel, G. Santiso-Quiñones, I. Krossing, *Chem. Eur. J.* **2009**, *15*, 1966–1976.
- [39] I. Krossing, *Chem. Eur. J.* **2001**, *7*, 490–502.
- [40] I. Krossing, A. Reisinger, *Coord. Chem. Rev.* **2006**, *250*, 2721–2744.
- [41] H. W. Roesky, D. K. Kennepohl, *Experiments in Green and Sustainable Chemistry*, Wiley-VCH, Weinheim, **2009**.
- [42] E. T. Mcbee, O. R. Pierce, H. W. Kilbourne, *J. Am. Chem. Soc.* **1953**, *75*, 4091–4092.
- [43] H. Millauer, W. Schwertfeger, G. Siegemund, *Angew. Chem.* **1985**, *97*, 164–182; *Angew. Chem. Int. Ed. Engl.* **1985**, *24*, 161–179.
- [44] A. Wroblewska, E. Milchert, E. Meissner, *Org. Process Res. Dev.* **2010**, *14*, 272–277.
- [45] I. Krossing, H. Brands, R. Feuerhake, S. Koenig, *J. Fluorine Chem.* **2001**, *112*, 83–90.
- [46] A. F. Holleman, E. Wieberg, N. Wieberg, *Lehrbuch der Anorganischen Chemie*, Walter de Gruyter, Berlin, **1995**, p. 127.
- [47] A. R. Choudhury, N. Winterton, A. Steiner, A. I. Cooper, K. A. Johnson, *J. Am. Chem. Soc.* **2005**, *127*, 16792–16793.
- [48] W. M. Reichert, J. D. Holbrey, R. P. Swatloski, K. E. Gutowski, A. E. Visser, M. Nieuwenhuyzen, K. R. Seddon, R. D. Rogers, *Cryst. Growth Des.* **2007**, *7*, 1106–1114.
- [49] K. Matsumoto, R. Hagiwara, R. Yoshida, Y. Ito, Z. Mazej, P. Benkic, B. Zemva, O. Tamada, H. Yoshino, S. Matsubara, *Dalton Trans.* **2004**, 144–149.
- [50] A. R. Choudhury, N. Winterton, A. Steiner, A. I. Cooper, K. A. Johnson, *CrystEngComm* **2006**, *8*, 742–745.
- [51] A. R. Choudhury, T. N. G. Row, *CrystEngComm* **2006**, *8*, 265–274.
- [52] O. Stenzel, H. G. Raubenheimer, C. Esterhuysen, *J. Chem. Soc. Dalton Trans.* **2002**, 1132–1138.
- [53] O. O. Okoturo, T. J. VanderNoot, *J. Electroanal. Chem.* **2004**, *568*, 167–181.
- [54] H. Rodríguez, J. F. Brennecke, *J. Chem. Eng. Data* **2006**, *51*, 2145–2155.
- [55] R. A. Carpio, L. A. King, R. E. Lindstram, J. C. Nardi, C. L. Hussey, *J. Electrochem. Soc.* **1979**, *126*, 1644–1650.
- [56] J. R. Sanders, E. H. Ward, C. L. Hussey, *J. Electrochem. Soc.* **1986**, *133*, 325–330.
- [57] K. R. Seddon in *Institute of Chemical Engineering and High Temperature Chemical Processes*, The International George Papatheodorou Symposium (Ed.: S. Boghosian), Patras, **1999**, p. 131.
- [58] A. R. Katritzky, R. Jain, A. Lomaka, R. Petrukhin, M. Karelson, A. E. Visser, R. D. Rogers, *J. Chem. Inf. Comput. Sci.* **2002**, *42*, 225–231.
- [59] F. H. Allen, *Acta Crystallogr. Sect. B* **2002**, *58*, 380–388.
- [60] H. D. B. Jenkins, H. K. Roobottom, J. Passmore, L. Glasser, *Inorg. Chem.* **1999**, *38*, 3609–3620.
- [61] H. D. B. Jenkins, J. F. Liebman, *Inorg. Chem.* **2005**, *44*, 6359–6372.
- [62] R. Ahlrichs, M. Baer, M. Haeser, H. Horn, C. Koelmel, *Chem. Phys. Lett.* **1989**, *162*, 165–169.
- [63] F. Weigend, M. Haeser, *Theor. Chem. Acc.* **1997**, *97*, 331–340.
- [64] A. Schaefer, C. Huber, R. Ahlrichs, *J. Chem. Phys.* **1994**, *100*, 5829–5835.
- [65] A. Klamt, G. Schüürmann, *J. Chem. Soc. Perkin Trans. 2* **1993**, *5*, 779–805.
- [66] A. Klamt, F. Eckert, *Fluid Phase Equilib.* **2000**, *172*, 43–72.
- [67] F. Eckert, A. Klamt, *AIChE J.* **2002**, *48*, 369–385.
- [68] P. Walden, *Z. Phys. Chem. (Leipzig)* **1906**, *55*, 207.
- [69] P. Walden, *Z. Phys. Chem. (Leipzig)* **1906**, *55*, 246.
- [70] W. Xu, E. I. Cooper, C. A. Angell, *J. Phys. Chem. B* **2003**, *107*, 6170–6178.
- [71] M. Yoshizawa, W. Xu, C. A. Angell, *J. Am. Chem. Soc.* **2003**, *125*, 15411–15419.
- [72] D. R. MacFarlane, M. Forsyth, E. I. Izgorodina, A. P. Abbott, G. Annat, K. Fraser, *Phys. Chem. Chem. Phys.* **2009**, *11*, 4962–4967.
- [73] K. J. Fraser, E. I. Izgorodina, M. Forsyth, J. L. Scott, D. R. MacFarlane, *Chem. Commun.* **2007**, 3817–3819.
- [74] W. Xu, C. A. Angell, *Science* **2003**, *302*, 422–425.
- [75] K. M. Johansson, E. I. Izgorodina, M. Forsyth, D. R. MacFarlane, K. R. Seddon, *Phys. Chem. Chem. Phys.* **2008**, *10*, 2972–2978.
- [76] A. B. Bourlino, K. Raman, R. Herrera, Q. Zhang, L. A. Archer, E. P. Giannelis, *J. Am. Chem. Soc.* **2004**, *126*, 15358–15359.

- [77] C. Daguinet, P. J. Dyson, I. Krossing, A. Oleinikova, J. M. Slattery, C. Wakai, H. Weingärtner, *J. Phys. Chem. B* **2006**, *110*, 12682–12688.
- [78] D. R. MacFarlane, K. R. Seddon, *Aust. J. Chem.* **2007**, *60*, 3–5.
- [79] H. Weingärtner, *Angew. Chem.* **2008**, *120*, 664–682; *Angew. Chem. Int. Ed.* **2008**, *47*, 654–670.
- [80] F. Kremer, A. Schönhals, *Broadband Dielectric Spectroscopy*, Springer, Berlin, **2003**.
- [81] C. Wakai, A. Oleinikova, M. Ott, H. Weingärtner, *J. Phys. Chem. B* **2005**, *109*, 17028–17030.
- [82] H. Weingärtner, *Z. Phys. Chem. (Muenchen Ger.)* **2006**, *220*, 1395–1405.
- [83] M.-M. Huang, H. Weingärtner, *ChemPhysChem* **2008**, *9*, 2172–2173.
- [84] R. Buchner, G. Hefter, *Phys. Chem. Chem. Phys.* **2009**, *11*, 8984–8999.
- [85] D. W. Davidson, R. R. Cole, *J. Chem. Phys.* **1951**, *19*, 1484–1490.
- [86] J. Hunger, A. Stoppa, S. Schrödle, G. Hefter, R. Buchner, *ChemPhysChem* **2009**, *10*, 723–733.
- [87] K. S. Cole, R. H. Cole, *J. Chem. Phys.* **1941**, *9*, 341–351.
- [88] M. N. Kobrak, H. Li, *Phys. Chem. Chem. Phys.* **2010**, *12*, 1922–1932.
- [89] C. Schröder, O. Steinhauser, *J. Chem. Phys.* **2009**, *131*, 114504/1–8.
- [90] P. J. Dyson, G. Laurency, C. A. Ohlin, J. Vallance, T. Welton, *Chem. Commun.* **2003**, 2418–2419.
- [91] R. C. Weast, *CRC Handbook of Chemistry and Physics*, CRS, London, **1972**.
- [92] C. L. Young in *IUPAC Solubility Data Series, Vols. 5–6*, Pergamon, Oxford, **1981**.
- [93] W. F. Linke, A. Seidell in *Solubilities of Inorganic and Metal–Organic Compounds, Vol. 1*, ACS, Washington, **1958**, p. 1075.
- [94] Precursors for the synthesis of the $[\text{Al}(\text{hfp})_4]^-$ ILs (both $[\text{Cat}]\text{X}$ salts ($\text{X} = \text{Cl}^-, \text{Br}^-$) and $\text{Li}[\text{Al}(\text{hfp})_4]$ salt) are commercially available by IoLiTec, Ionic Liquids Technologies, <http://www.iolitec.de>.
- [95] G. Laurency, P. J. Dyson, *Z. Naturforsch. B* **2008**, *68*, 681–684.
- [96] CCDC 794464 (1), 794463 (2), 794465 (3), 794468 (4), 794466 (6), and 794467 (9) contain the supplementary crystallographic data for this paper. These data can be obtained free of charge from The Cambridge Crystallographic Data Centre via www.ccdc.cam.ac.uk/data_request/cif

Received: April 16, 2010
Published online: September 30, 2010